

TOPICAL REVIEW • OPEN ACCESS

Design and manufacturing of micro/nanorobots

To cite this article: Junmin Liu *et al* 2024 *Int. J. Extrem. Manuf.* **6** 062006


View the [article online](#) for updates and enhancements.

You may also like

- [Performance-control-orientated hybrid metal additive manufacturing technologies: state of the art, challenges, and future trends](#)
Jiming Lv, Yuchen Liang, Xiang Xu et al.
- [Review on laser directed energy deposited aluminum alloys](#)
Tian-Shu Liu, Peng Chen, Feng Qiu et al.
- [Recent progress in bio-inspired macrostructure array materials with special wettability—from surface engineering to functional applications](#)
Zhongxu Lian, Jianhui Zhou, Wanfei Ren et al.

Topical Review

Design and manufacturing of micro/nanorobots

Junmin Liu^{1,2,3}, Rencheng Zhuang^{1,2,3}, Dekai Zhou^{1,2,3}, Xiaocong Chang^{1,2,3,*} and Longqiu Li^{1,2,3,*} 

¹ State Key Laboratory of Robotics and System, Harbin Institute of Technology, Harbin, People's Republic of China

² Key Laboratory of Micro-systems and Micro-structures Manufacturing, Harbin, People's Republic of China

³ Zhengzhou Research Institute of Harbin Institute of Technology, Zhengzhou, People's Republic of China

E-mail: xiaocong@hit.edu.cn and longqiuli@hit.edu.cn

Received 15 May 2024, revised 7 July 2024

Accepted for publication 21 August 2024

Published 4 September 2024



Abstract

Micro/nanorobots (MNRs) capable of performing tasks at the micro- and nanoscale hold great promise for applications in cutting-edge fields such as biomedical engineering, environmental engineering, and microfabrication. To cope with the intricate and dynamic environments encountered in practical applications, the development of high performance MNRs is crucial. They have evolved from single-material, single-function, and simple structure to multi-material, multi-function, and complex structure. However, the design and manufacturing of high performance MNRs with complex multi-material three-dimensional structures at the micro- and nanoscale pose significant challenges that cannot be addressed by conventional serial design strategies and single-process manufacturing methods. The material-interface-structure-function/performance coupled design methods and the additive/formative/subtractive composite manufacturing methods offer the opportunity to design and manufacture MNRs with multi-materials and complex structures under multi-factor coupling, thus paving the way for the development of high performance MNRs. In this paper, we take the three core capabilities of MNRs—mobility, controllability, and load capability—as the focal point, emphasizing the coupled design methods oriented towards their function/performance and the composite manufacturing methods for their functional structures. The limitations of current investigation are also discussed, and our envisioned future directions for design and manufacture of MNRs are shared. We hope that this review will provide a framework template for the design and manufacture of high performance MNRs, serving as a roadmap for researchers interested in this area.

Keywords: micro/nanorobots, functional structure, design, manufacturing

* Authors to whom any correspondence should be addressed.



Original content from this work may be used under the terms of the [Creative Commons Attribution 4.0 licence](https://creativecommons.org/licenses/by/4.0/). Any further distribution of this work must maintain attribution to the author(s) and the title of the work, journal citation and DOI.

1. Introduction

Micro/nanorobots (MNRs) can convert other forms of energies in the environment (e.g. optical [1–4], ultrasonic [5–8], electrical [9–11], magnetic [12–16]) into their own kinetic energy, and can self-drive [17, 18], sense [19–21], transport [22–24] and micro-manipulate [25, 26] in liquid-phase medium, and hence, show great potential to be used in the fields of biomedical sciences [27–30], micro- and nano-processing [31, 32] and environmental engineering [33–36]. In the last decade or so, MNRs have made significant advances in materials, driven, control and manufacturing technologies. Materials ranging from metals (e.g. Pt [37], Ir [38]), polymers (e.g. poly(lactic-co-glycolic acid) [39], poly(3,4-ethylenedioxythiophene) [40]) to biomaterials (e.g. spore [12], urease [41]) have been used for MNRs with different functional requirements. Chemical [42, 43], ultrasonic [44, 45], optical [46, 47], electric [48, 49] and magnetic fields [50, 51], as well as their mixed fields [52–54], also play an important role in the driving and controlling of MNRs. Numerous manufacturing methods have also been employed for MNRs, such as physically based (physical vapor deposition (PVD) [55, 56], direct laser writing (DLW) [57, 58], microfluidic synthesis [59, 60], etc) and chemically based (template electrodeposition (TAE) [61, 62], wet chemical etching (WCE) [63, 64], layer-by-layer (LbL) self-assembly [65, 66], etc). Advances in materials science and nanotechnology have led to the design and manufacture of a wide variety of MNRs. These MNRs have similar core capabilities such as mobility, controllability and load capability. These capabilities serve as the basis for MNRs to perform a wide range of tasks. MNRs with more capabilities can be defined as high capability MNRs. The degree to which an MNR achieves a particular capability is referred to as performance. For example, the mobility performance of an MNR mainly refers to the magnitude of its attainable speed. Thus, high performance MNRs are advanced manifestations of high capability MNRs. They can achieve a variety of capabilities to a high degree. These enhanced performances are crucial for MNRs to achieve their tasks in complex environments. Therefore, the design and manufacturing of high performance MNRs are imperative.

To navigate and accomplish tasks in intricate and dynamic environments, high performance MNRs frequently necessitate the fusion of multiple materials (e.g. metal material [67, 68], smart materials [69, 70], composite materials [29, 71]), the construction of complex structures (e.g. asymmetric structures [49, 72, 73], rigid-flexible coupled structures [57, 74, 75], deformation structures [76, 77]), and the integration of multiple functions (e.g. mobility [78–80], controllability [81–83], cargo transportation capability [84–86]) at the micro- and nanoscale. However, these demands bring many challenges to the design and manufacturing of high performance MNRs. Firstly, it is difficult to achieve the design of high performance MNRs with conventional serial and isolated design strategies due to the complexity of the effects

caused by multi-material distribution, surface/interface properties, and cross-scale structural features on their performance. Secondly, a single manufacturing technology is insufficient to meet the highly integrated manufacturing requirements of complex multi-material three-dimensional (3D) structures for high performance MNRs at the micro- and nanoscale.

The material-interface-structure-function/performance coupled design methods and the additive/formative/subtractive composite manufacturing (AFS-CM) methods are the key to overcoming the design and manufacturing challenges of high performance MNRs. However, material selection, structural design, process control, and function/performance realization of MNRs are often empirical and isolated, lacking basic science theories to guide a systematic approach. Therefore, to customize high performance MNRs for specific tasks requires a complete fundamental understanding of the basic science behind the materials/interfaces/structures/processes and functions/performances of MNRs.

As a typical cross-discipline, MNRs have rich scientific and technological connotations in terms of material [87–91], structure [92–96], process [97–101], function/performance [102–106] and related applications [107–113]. Several other excellent reviews deal with recent advances in each of these areas. Unfortunately, these reviews mainly emphasize the propulsion mechanisms, structures, fabrication techniques or applications of MNRs, while ignoring the fundamental scientific framework of their design and manufacturing processes. Therefore, we do not address these aspects separately, but instead propose a holistic concept of ‘Function/performance-oriented design and manufacturing of MNRs’. The objective is to provide a scientific paradigm for the design and manufacture of high performance MNRs. Taking the three core capabilities of MNRs as the starting point, we highlight the impact of material/interface/structure on function/performance, show how structure-function/performance integrated MNRs can be manufactured utilizing AFS-CM method, and envision future integrated systems for design and manufacture.

This paper reviews the design and manufacturing methods of high performance MNRs, as shown in figure 1. The coupled design methods for high performance MNRs are discussed in section 2. In this section, we focus on three main areas, including material-function integrated design, interface-performance integrated design, and structure-performance integrated design. In section 3, based on different manufacturing characteristics, we categorize manufacturing methods into three categories, including additive manufacturing, formative manufacturing, and subtractive manufacturing, and summarize the existing manufacturing methods. In addition, we address in detail composite manufacturing methods for functional structures of existing MNRs. Finally, in section 4, we discuss the limitations of the current investigations, envision possible future design methods, manufacturing processes, and testing techniques, and demonstrate

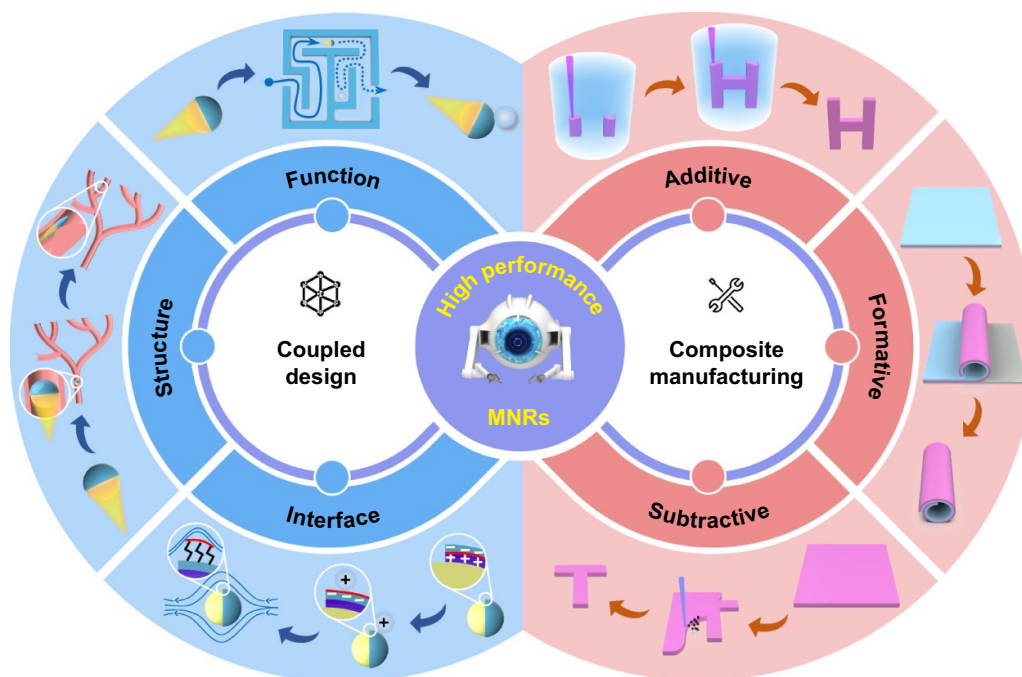


Figure 1. Summary of design and manufacturing methods of high performance MNRs.

future integrated systems for design, manufacturing, and testing.

2. Coupled design methods

Design stands as the linchpin in the development of MNRs. It encompasses various aspects such as stability, environmental adaptability, and functionality of MNRs, exerting a significant impact on the choice of materials and manufacturing processes. Consequently, the scientific and rational nature of the design directly correlates with the success or failure of MNRs research and development. Central to the design process is the strategic selection and distribution of materials, the optimization of multi-scale interfaces, and the careful choice of structural features. Thus, achieving high performance MNRs necessitates the coupled design approach that integrates considerations of materials, interfaces, and structures (figure 2).

2.1. Material-function integrated design

How to realize motion in low Reynolds number environments, how to realize response control in complex environments, and how to realize high loads at the micro- and nanoscale are essential to consider when designing MNRs. Therefore, MNRs should have functions such as mobility, controllability and load capability. These functional modules are the basis and core of the functional framework for building MNRs. To design the functional modules of MNRs at the micro- and nanoscale, the selection and matching of materials is crucial. From inorganic materials, organic materials to biological materials, the inherent properties of materials are the main

reason why they are chosen to build MNRs. Taking the function/performance of MNRs as the core, adopting the design ideology of material-function integrated is an important way to break through the technological bottleneck of MNRs, such as the difficulty of motion, control, and loading in low Reynolds number environments/micro- and nanoscale. Here, we focus on the design of mobility, controllability, and load capability of MNRs.

2.1.1. Mobility. Mobility is an important feature to distinguish MNRs from passive particles. MNRs can be driven by endogenous and exogenous stimuli. The power of endogenously driven MNRs can be provided by catalytic materials or self-fuels (such as Zn [114], Mg [115], Al [116]) incorporated into the material system of MNRs. Among them, the types of catalytic materials are very rich, including inorganic materials such as Ir [38] (figure 3(a)), Pt [83], MnO₂ [117] that can catalyze the decomposition of chemical fuels (such as N₂H₄ [38], H₂O₂ [117]), and biopolymer materials that can provide higher biocompatibility (such as glucose oxidase [118], urease [119]). In addition, biological hybrid strategies can also be used to use organisms with autonomous movement capabilities (such as *Escherichia coli* [120], *Chlamydomonas reinhardtii* [121], etc) as the power source of MNRs. The power of exogenously driving MNRs is provided by external physical fields such as light, electricity, magnetism, and ultrasound. To design MNRs with external physical field propulsion capabilities, it is necessary to introduce light-responsive materials [80, 122], conductive materials or dielectric materials [123, 124], magnetic materials [125, 126], etc into MNRs, or to distribute materials non-uniformly (such as choosing two materials with different densities [127]).

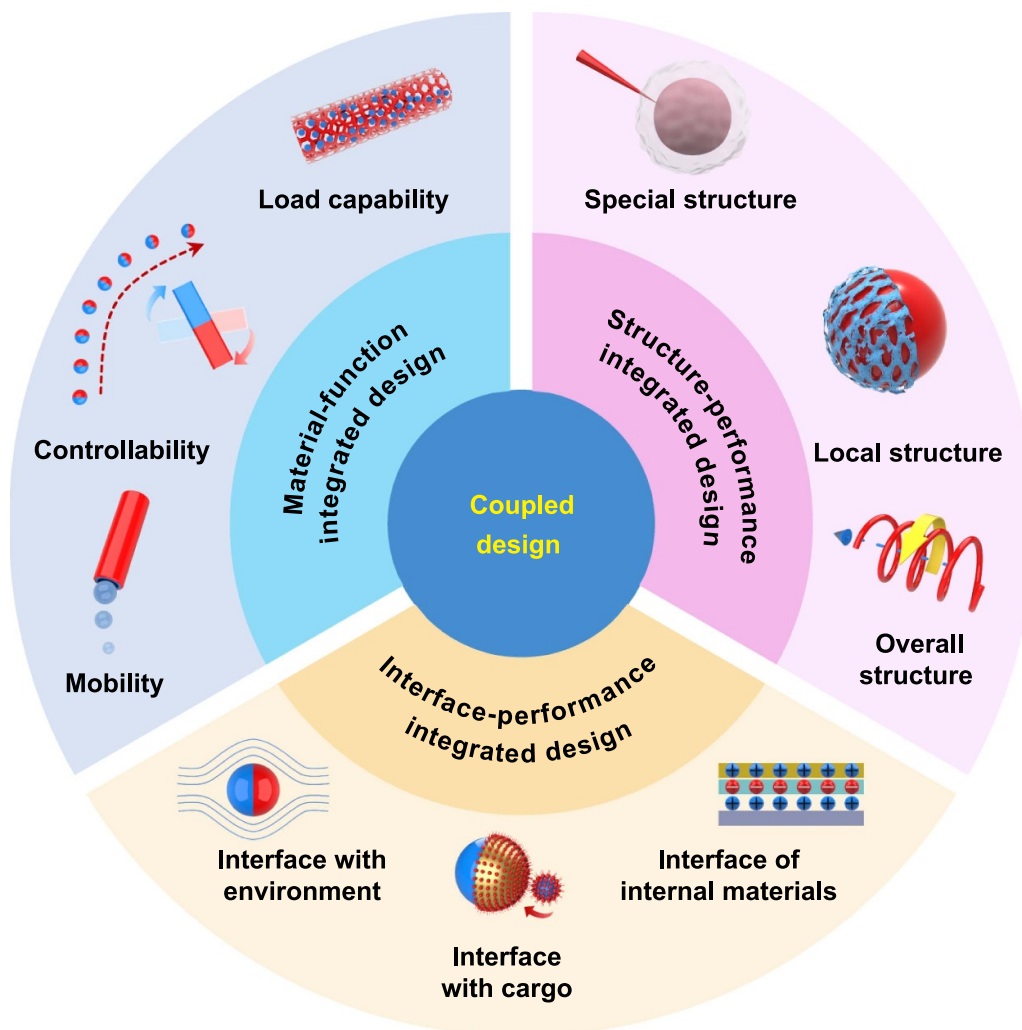


Figure 2. Summary of the multi-material and structure matched multi-functional/high performance design of MNRs.

2.1.2. Controllability. In order to improve the flexibility of MNRs to perform complex tasks, excellent controllability is necessary. Precise directional control is an important embodiment of controllability. Compared with the lack of directionality in the motion control of MNRs by ultrasonic or chemical fields, and the limitations of the application of light and electric fields in some fields, the motion control of MNRs by magnetic fields has excellent directionality and environmental friendliness. Therefore, adding magnetic materials (such as Fe [1], Ni [128], Co [129], Fe_3O_4 [130, 131] (figure 3(b))) to the designed MNRs to make them controllable by a magnetic field is of great significance for improving the controllability of the MNRs. When combined with medical imaging feedback, MNRs enable real-time autonomous navigation in complex dynamic biological environments, providing an intelligent approach to automated drug delivery *in vivo* [132–134]. In addition, by modifying specific aptamers on MNRs, MNRs can also obtain more advanced autonomous targeting capabilities, such as specific antibodies [135], specific DNA [136], etc. Furthermore, smart materials are able to sense external stimuli and respond appropriately. This opens up new possibilities for the diversified controllability of MNRs.

For example, azobenzene [69], spiropyran [70], and poly(N-isopropylacrylamide) [137].

2.1.3. Load capability. Load capability relates to how much functional material can be loaded into an MNR, and it can affect the efficiency of functional expression. The specific surface area is an important parameter for measuring the load capability of a material, and materials with a large specific surface area usually have higher load capability. Therefore, materials with high specific surface area, such as one-dimensional or two-dimensional (2D) nanomaterials (graphene oxide (GO) [138], reduced graphene oxide [139], black phosphorus [140], MoS_2 [141], and WS_2 [142]), micro-clay minerals (montmorillonite [143], zeolite [144], and halloysite nanotube (figure 3(c)) [86]), organic framework materials (ZIF-90, ZIF-8, MOF-5, etc [145]) and some synthetic porous hollow materials [146, 147], are ideal for enhancing the load capability of MNRs. In addition, it is necessary to consider how the load of the MNR will be released. There are two typical methods of release load. One is to use external physical fields to control the corresponding changes in the

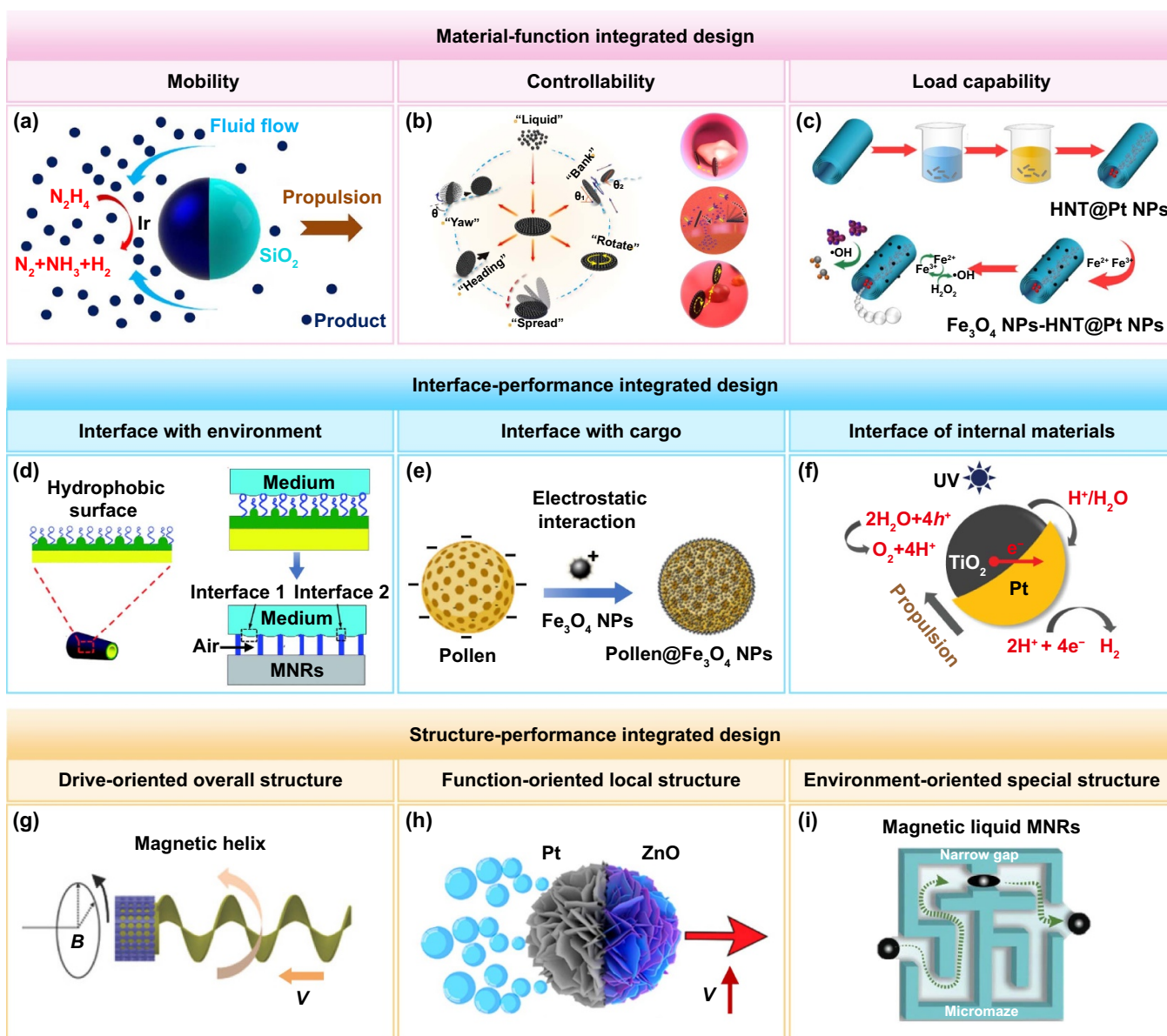


Figure 3. Coupled design of high performance MNRs. (a) Schematic of catalytic Ir/SiO₂ Janus microrobots powered by hydrazine. Reprinted (adapted) with permission from [38]. Copyright (2014) American Chemical Society. (b) Multiple switchable motion modes for Fe₃O₄ NPs cluster. Reprinted (adapted) with permission from [131]. Copyright (2022) American Chemical Society. (c) Schematic of the preparing of Fe₃O₄ NPs-HNTs@Pt NPs. Reprinted (adapted) with permission from [86]. Copyright (2021) American Chemical Society. (d) Ultrafast propulsive tubular MNR with hydrophobic surface. Adapted from [151] with permission from the Royal Society of Chemistry. (e) Enhanced load capability using electrostatic interactions. Reprinted (adapted) with permission from [154]. Copyright (2022) American Chemical Society. (f) Interfacial electron transfer within Pt/TiO₂ Janus MNRs materials [80]. John Wiley & Sons. © 2020 WILEY-VCH Verlag GmbH & Co. KGaA, Weinheim. (g) Magnetically driven helical microrobot [172]. John Wiley & Sons. © 2018 WILEY-VCH Verlag GmbH & Co. KGaA, Weinheim. (h) Surface microstructure enhances motion performance. Reprinted (adapted) with permission from [177]. Copyright (2018) American Chemical Society. (i) Liquid MNRs for navigation in complex environments [184]. John Wiley & Sons. © 2020 WILEY-VCH Verlag GmbH & Co. KGaA, Weinheim.

corresponding response materials to achieve load release. For example, near-infrared light is used to stimulate photothermal materials (such as Au, indocyanine green) to release heat, and then the materials such as gelatin hydrogel or liposomes carrying cargo are cracked to release the cargo [125, 148]. The other is to use the microenvironmental characteristics of the target site to cleave the corresponding response material to release the loading, such as using the acidic environment of the

target site to crack the acid-degradable material to release the load [149].

2.2. Interface-performance integrated design

The construction of the functional framework of MNRs can be realized by the rational selection of materials. On this basis, how to realize low resistance motion in low Reynolds number

environment, how to realize efficient and stable loading of loads, and how to realize multi-material compatibility are the problems that must be faced in designing high performance MNRs. The interfaces between the MNRs and environment and their loads, as well as the interfaces between their internal materials, directly affect the expression of their functions such as mobility, load capability and stability. Therefore, based on the performance of MNRs, the interface-performance integrated design philosophy can promote the MNRs to leap forward to high performance. Here, we discuss the interfaces between MNRs and the environment, the interfaces with loads, and the interfaces within the materials from three perspectives, namely, ‘macro’, ‘micro’, and ‘nano’.

2.2.1. Interface with environment. In low Reynolds number environments, inertial forces are negligible, however, the effect of viscous forces is more significant. And the magnitude of the viscous force is influenced by the interface constructed between the MNR and the environment. By designing the wettability of the interface of MNRs in contact with the environment to form a superhydrophobic surface, their kinematic performance can be substantially improved [150]. The principle is that the superhydrophobic surface can partially transform the solid–liquid contact interface between the MNR and the liquid environment into a gas–liquid contact interface, and will generate a considerable velocity slip on the interface, thus significantly reducing the drag force of the MNR in motion, so as to achieve the effect of increasing the velocity. There are two ways to construct hydrophobic surfaces for MNRs, either by constructing rough microstructures or by coating them with low surface energy materials, or by combining the two (figure 3(d)) [151]. In addition, in the face of increasingly complex environments, rationally constructing the interface between MNRs and their environments is also an important way to enhancing their stability and controllability. For example, by designing an enterosoluble mucous membrane on the surface of the MNR, high stability can be achieved as it passes through the highly acidic environment of the stomach. It is also possible to control its movement distance in the intestine by controlling the thickness of the membrane [68]. In addition, constructing a biological surface by wrapping a biofilm around the MNR can realize the biological camouflage of the MNR and improve its environmental adaptability and ability to perform tasks [152].

2.2.2. Interface with cargo. Unlike the macroscopic scale, MNRs are loaded by surface modification. Therefore, the load capability of the MNR can be enhanced by designing the way of combining it with loads. Loads are combined with MNRs in two main ways: physical adsorption and chemical bonding. Physical adsorption mainly uses the weak connection between materials to bind materials together, such as van der Waals force [153], electrostatic interaction between charged materials (figure 3(e)) [19, 154], hydrogen bond [130], hydrophobic interaction [155], π – π stacking [139], etc. For example, through electrostatic interactions,

positively charged MNRs loaded negatively charged citrate-coated gold nanoparticles (NPs), which endowed the MNRs with more active sites [19]. Hydrogen bond has been used to load polyvinylpyrrolidone-coated Fe_3O_4 NPs onto the surface of gelatin methacryloyl hydrogel microstructures [130]. In contrast to physical adsorption, chemical bonding is achieved by establishing covalent, metallic, or ionic bonds between the MNRs and the load in order to form strong chemically bonded interfaces for load loads. One of the most widely used methods is the construction of covalently bonded interfaces using chemical linkers, especially when the MNRs or the loads are biological materials. This method not only greatly improves the efficiency of load attachment, but also brings the desired selectivity to its immobilization and separation processes. Commonly used chemical linkers include 1-ethyl-3-(3-dimethylaminopropyl) carbodiimide – N-hydroxysuccinimide [156, 157], biotin systems [158, 159] and pentanediol [146]. For example, using pentanediol as the chemical linker, various biological enzymes can be loaded onto the surface of MNRs [146].

2.2.3. Interface of internal materials. The functional integration of MNRs relies on the combination of multiple functional materials. Therefore, the compatible matching between multi-materials is crucial for the stability and functional expression of MNRs. When designing MNRs, their stability can be improved by matching materials appropriately. For example, by adding Ti materials between metals (Ni [81]) or metal oxides (TiO_2 [160]) and SiO_2 substrates, the interfacial energy between the materials can be significantly reduced, leading to enhanced inter-material bonding and stability of the MNRs. In addition, the kinematic performance of MNRs can be enhanced by material matching. For example, compared to metals such as Cu, Fe, Ag, Au, etc, Janus spherical MNRs composed of Pt and TiO_2 exhibit enhanced kinematic properties, which is attributed to superior chemical potential and catalytic synergies (figure 3(f)) [80]. And interfacial electron transfer can be enhanced by adding GO to the surface of Cu_2O -based MNRs, thus dramatically increasing their motion speed [161]. In addition, the combination of materials within MNRs is based on physical adsorption or chemical bonding. For example, materials that are combined by thermal spraying, coating, or hot pressing have interfacial forces between the materials that are predominantly van der Waals forces. Interfaces between oppositely charged materials are usually built by electrostatic interaction. In contrast, PVD, atomic layer deposition (ALD) and TAE are all multi-material interfaces built through chemical bonding.

2.3. Structure-performance integrated design

Drag forces proportional to feature lengths have a significantly greater impact on MNRs than inertial forces at the micro- and nanoscale due to size effects. Therefore, compared to enhancing the mobility performance of MNRs by designing their interfaces with environment, the enhancement of their mobility performance by rationally designing their

overall/local structures is more significant. In addition, choosing appropriate drive methods for different overall structures, designing appropriate local structures for different functions, and designing special structures for different application environments are also important ways to enhance the performance of MNRs. Therefore, adopting a function/performance-oriented, structure-performance integrated design philosophy for MNRs can further enhance their task performance abilities, such as mobility, load capability, and environmental adaptability.

2.3.1. Drive-oriented overall structure. Spheres, rods, tubes and helices are the most commonly used overall structures for MNRs [162]. Spheres have the smallest surface potential and are the easiest structures to synthesize. Spherical MNRs have no corners and have high environmental adaptability, allowing them to perform tasks in complex environments without compromising their motion. In low Reynolds number environments, breaking the symmetry of motion is the prerequisite for MNRs to obtain mobility. Due to the special symmetry of spheres, asymmetric MNRs can be mass-produced by adding or removing material asymmetrically without having to choose the orientation. Spherical MNRs are suitable for almost any drive method, and the most commonly used drive methods are chemical [163], optical [164], magnetic [165], and electric [10]. Rods are another easy-to-fabricate structure. During manufacture, rods can be easily asymmetric by arranging different materials along the axial or radial direction. The common driving methods for rod-shaped MNRs are chemical [166], optical [167], ultrasonic [73], magnetic [67] and electric [168]. In addition, rod-shaped MNRs can be designed to be flexible, allowing for richer motion patterns [169]. Moreover, compared to spheres, rods have high aspect ratios that are more favorable for them to perform some special tasks, such as their rotational motion along the radial direction that can be used for biochemical release [170]. Tubular structures are preferred for bubble-driven MNRs because their internal hollow structure facilitates bubble generation and release [171]. Tubes can be designed as straight or tapered. Compared to straight tubes, tapered tubes not only experience less drag during motion, but also allow for the directional release of bubbles in response to the ultrasonic field [66]. In addition, the internal space of the tube can be used to load cargo, thus providing an advantage over rods and spheres for cargo transport [68]. Due to the excellent mobility in the rotating magnetic field, helices are often used as the overall structure for magnetically driven MNRs (figure 3(g)) [172]. In addition, the helical propulsion of the helical MNRs in the rotating magnetic field gives them a strong cell-penetration capability [173, 174]. In addition, the space inside the helix allows for excellent cargo capture and transport capabilities, such as the capture and transport of sperm [175].

2.3.2. Function-oriented local structure. The performance of various functions of MNRs can also be enhanced by designing their local structures. The motion performance of MNRs

can be improved by designing the microstructure surfaces. There are three main intrinsic mechanisms, the first of which is to increase the contact area between the catalytic material and the fuel in the medium environment through the surface microstructure, which in turn enhances the catalytic efficiency and thus the motion performance of the MNRs (figure 3(h)) [176, 177]. The second one is to enhance the motion performance of MNRs by enhancing the interfacial charge transfer through surface microstructures and hindering the electron-hole combination rate, which in turn enhances the photoresponsive properties [178]. The third one utilizes the high specific surface area characteristics of surface microstructures to enhance the load capability of MNRs, which in turn can be loaded with more biological enzymes, thus enhancing the motion performance of MNRs [41]. Besides surface microstructures, the load capability [179] or cargo capture capability [34] of MNRs can be significantly improved by designing hollow or lattice structures. In addition, MNRs can also be engineered to perform specific functions by designing surface microstructures, e.g. neuronal growth can be aligned and guided by engineered surface groove microstructures [180].

2.3.3. Environment-oriented special structure. When faced with unique environments or specific application requirements, designing specialized structures can often enhance the effectiveness of MNRs. For instance, in applications where MNRs need to withstand specific pressures, such as cell puncture [174, 181] or breaching mucous membranes [82, 182], structures with high aspect ratios and pointed tips are more conducive to fulfilling their tasks. Flexible MNRs offer outstanding advantages over rigid MNRs in adapting to unpredictable environments, such as in restricted, hard-to-reach tissues and blood vessels in the body. Flexible MNRs can be obtained by integrating flexible components that act as hinges or tails on rigid MNRs [74, 169, 183]. These flexible components are generally made of soft metallic or polymeric materials. They can break the spatial and temporal symmetry under the action of external fields thus allowing MNRs to obtain more flexible motion. In addition, flexible chains consisting of multiple rigid segments and joints have been proposed to reduce the complexity of manufacturing and to circumvent the challenges posed by the interface between rigid and flexible components [57]. Liquid MNRs are an important branch of flexible MNRs, such as magnetic liquid microrobots (figure 3(i)) [184], and liquid metal microrobots [185]. They have excellent environmental adaptability as they are able to actively deform when encountering narrow spaces. In addition, smart materials are often used to build flexible MNRs. These smart materials are capable of morphological transitions in response to environmental changes (e.g. pH [186], temperature [137]) or external stimuli (e.g. light [77]), providing new ideas for functional integration of MNRs. For example, flexible hookworm-shaped MNRs using smart materials can load or release cargo in a more controlled manner [187].

2.4. Summary

As the application scenarios of MNRs change, higher demands are placed on the complex environmental adaptability and functionality of MNRs. By taking functional requirements and functional expression as the core, the design concept of combining functional design, interfacial design and structural design provides a new way and breakthrough for high performance MNRs with high environmental adaptability, excellent stability and functional diversity. Table 1 shows typical examples of MNRs based on material-interface-structure-function/performance coupled design. However, in order to realize the multiple functions of MNRs, the choice of multiple materials often increases the difficulty and complexity of manufacturing, and increases the uncertainty of functional expression. Therefore, it is necessary to explore new materials that can realize multiple functions, so as to simplify the design and manufacture of MNRs and reduce the risk of functional failure of MNRs. In addition, existing interfacial binding methods suffer from poor stability. Designing and constructing multi-material interfaces in a highly controllable manner remains a challenge for various environments. This process necessitates the secure bonding of varied functional materials while preserving their intrinsic properties and functionalities.

3. Composite manufacturing methods

Manufacturing stands as the linchpin in realizing the design intricacies of MNRs. With the evolution of nanotechnology, the array of manufacturing methods and functionalization strategies for MNRs has undergone considerable diversification, encompassing techniques. Broadly classified, manufacturing methods fall into three primary categories: additive manufacturing, formative manufacturing, and subtractive manufacturing [196, 197]. In contrast to macroscopic scales, which often rely on subtractive manufacturing, MNRs utilize a composite manufacturing method primarily based on additive manufacturing, combining formative and subtractive techniques (figure 4). This section will review the manufacturing methods of MNRs, followed by a discussion of the composite manufacturing of each functional structure. The structures include Janus spheres, rods, tubes, helices, and some unique structures, and are all analyzed from a material/structure/function/performance/process perspective.

3.1. Overview of manufacturing methods for MNRs

Additive manufacturing is a method of creating desired structures by adding materials [198–201]. In accordance with material-function integrated design, various functional materials are incorporated during the manufacturing process to impart different functionalities to MNRs. For example, the addition of magnetic metallic materials can provide MNRs with magnetic propulsion and guidance to MNRs [202], and the addition of enzymes can provide MNRs with mobility

[203]. Therefore, additive manufacturing method is the preferred manufacturing method for MNRs. MNRs of various sizes and shapes have been fabricated using various types of additive manufacturing methods, ranging from liquid phase deposition (e.g. LbL self-assembly [204, 205]) and vapor phase deposition (e.g. PVD [206, 207], ALD [208, 209]), which can provide MNRs with 2D functional material coatings, to electrochemical (e.g. electrochemical deposition [210, 211]) and photopolymerization fabrication methods (e.g. microfluidic synthesis [212, 213], DLW [214, 215]) that can generate 3D micro- and nanostructures, to multidimensional biological hybrid fabrication technologies (e.g. biomolecule hybrids [216, 217], biofilm hybrids [218, 219], biobody hybrids [220, 221]) (figure 5). In contrast to additive manufacturing methods that require the addition of materials to fabricate asymmetric structures, formative manufacturing methods utilize stimuli within the material (e.g. strain, elasticity) or stimuli from the external environment (e.g. solvent evaporation, temperature, pressure, etc) for the purpose of fabricating MNRs with a specific structure, such as self-rolled [222, 223] and phase separation [224, 225]. Subtractive manufacturing is a process of creating structures with desired shapes and sizes by removing material. This can be achieved through various methods such as dry etching [226], WCE [72, 227], and femtosecond laser ablation [26, 153].

Table 2 lists the minimum feature sizes for the manufacturing methods described above, as well as the typical size ranges, typical structures, typical materials, production scales, advantages, and disadvantages of MNRs oriented. Due to the different principles, there are significant differences in the range of molding sizes, applicable shapes, and production scales among the various manufacturing methods for MNRs. And all of them have their unique advantages, but inevitably have disadvantages. Therefore, the AFS-CM method has become an important technological pathway to fabricate highly integrated functional structures for high performance MNRs. This method combines the advantages of additive, formative, and subtractive manufacturing methods. Miskin *et al* proposed a composite manufacturing method for sub-hundred-micron walking robots that combines ALD, PVD, self-rolled, WCE, and dry etching [228]. The fabricated MNRs are capable of optical-electrical-mechanical energy conversion and will significantly advance the intelligence of MNRs due to their compatibility with standard CMOS processing.

3.2. Janus spherical MNRs

The Janus sphere is an asymmetric structure with different physical or chemical properties in its two hemispheres, allowing it to break kinematic symmetry and acquire mobility properties. It is important to note that its asymmetry is primarily achieved by multi-material distribution. Depending on how the materials are distributed, it can be classified as a volume divided Janus sphere or a surface divided Janus sphere. Figure 6 shows two types of Janus spheres and their manufacturing methods, as well as the methods of obtaining functional materials.

Table 1. Typical cases of material-interface-structure-function/performance coupled design for MNRs.

Function	Category	Material	Components	Interface and performance	Propulsion mechanism	Structure	References
Mobility	Self-fuel	Mg	Mg/Ti/Ni/Au	<ul style="list-style-type: none"> Ti enhances Mg and Ni bonding 	Chemical	Janus sphere	[188]
		Zn	Zn/Fe/Poly(aspartic acid)/DOX	<ul style="list-style-type: none"> Poly(aspartic acid) and DOX form electrostatic interaction interface Enhanced load capability 	Chemical	Tube	[82]
Catalyst		Al	Al/Ga/Ti	<ul style="list-style-type: none"> Ga prevents Al from forming oxide passivation layer Enhanced propulsion efficiency 	Chemical	Janus sphere	[189]
		Pt	Pt/WS ₂	<ul style="list-style-type: none"> Rough surface of WS₂ Enhanced motion performance and load capability 	Chemical	Tube	[142]
		ZnO	ZnO/Pt	<ul style="list-style-type: none"> The surface microstructure of ZnO enhances the charge transfer between the Pt and ZnO interfaces, reduces the electron-hole recombination rates Significantly improves the kinematic properties 	Optical	Janus sphere with surface microstructure	[176]
Organism		Urease	SiO ₂ /Urease	<ul style="list-style-type: none"> Urease is loaded through chemical linkers 	Chemical	Hollow mesoporous Janus sphere	[119]
		Chlamydomonas reinhardtii (CR)	CR	<ul style="list-style-type: none"> Biocompatible surfaces 	Biological	Double flagellum	[121]
		<i>E. coli</i> (<i>E. coli</i>)	<i>E. coli</i> -PS(PAH/PSS) ₄ PAH@Fe ₃ O ₄	<ul style="list-style-type: none"> Affinity surface loading <i>E. coli</i> 		Spheroid-bound <i>E. coli</i>	[120]
		Spermatozoa	Spermatozoa/ZIF-8	<ul style="list-style-type: none"> ZIF-8 loaded on the surface of spermatozoa by chemical linker 		Single flagellum	[190]

(Continued.)

Table 1. (Continued.)

Function	Category	Material	Components	Interface and performance	Propulsion mechanism	Structure	References
Controllability	Magnetic materials	Fe	SiO ₂ /Au/Ti/Fe/Au	<ul style="list-style-type: none"> Ti enhances Au and Fe bonding 	Optical	Janus sphere	[1]
		Co	Sunflower pollen/Au/Co/Au	<ul style="list-style-type: none"> Au interface traps cancer cells through electrostatic interactions 	Magnetic	Janus sphere	[129]
Smart materials		Fe ₃ O ₄	GelMA-Fe ₃ O ₄ NPs	<ul style="list-style-type: none"> Fe₃O₄ NPs loading through hydrogen bonded interfaces 	Magnetic	Soft helix	[130]
		Azobenzene	Hollow mesoporous SiO ₂ -Azobenzene/Pt@β-CD	<ul style="list-style-type: none"> The azobenzene forms a host-guest interaction interface with β-CD Photoisomerization of the azobenzene leads to the rapid disassembly of β-CD 	Chemical	Hollow mesoporous sphere	[69]
Controllability	Bio-materials	Cys-Arg-Glu-Lys-Ala (CREKA) peptide	PDA@CREKA	<ul style="list-style-type: none"> CREKA loaded via covalent bonds and provide targeting capability 	Optical	Hollow asymmetric sphere	[191]
		Anti-HER2	SiO ₂ /Ni/Au@Anti-HER2	<ul style="list-style-type: none"> Anti-HER2 loaded via chemical linker and provide targeting capability 	Magnetic	Janus sphere	[135]
Load capability		MSR-1	MSR-1-DOX	<ul style="list-style-type: none"> Biocompatible surfaces Provides drive and directional control capabilities 	Biological	Foliated	[192]
	1D or 2D nanomaterials	rGO	rGO/Pt/Specific ricin B aptamer@Fluorescein-amidime (FAM)	<ul style="list-style-type: none"> rGO and FAM form π-π stacked interfaces with fluorescence quenching Specific ricin B aptamer and Specific ricin B specific binding, fluorescence on 	Chemical	Tube	[139]
		Carbon nanotube (CNT)	CuO ₂ /N-CNT	<ul style="list-style-type: none"> N-CNT forms charge migration interface with CuO₂ and hinders charge recombination Enhanced photocatalytic activity and motion performance 	Chemical	Tube	[193]

(Continued.)

Table 1. (Continued.)

Microclay minerals	Montmorillonite	Montmorillonite/Pt	Modified montmorillonite forms hydrophobic surface	Chemical	Janus sphere	[143]
	Halloysite Nanotube (HNT)	HNT@Pt NPs@Fe ₃ O ₄ NPs	<ul style="list-style-type: none"> Enhanced cargo loading capability HNT internal and external surfaces have non-homogeneous properties Enhanced cargo loading versatility 	Chemical	Tube	[86]
Organic framework materials	Azine-linked covalent organic framework (Py-Azine COF) Spore	PCL/Py-Azine COF-Fe ₃ O ₄ -MnO ₂	<ul style="list-style-type: none"> Py-Azine COF forms hydrogen bonds with 2,4,6-trinitrophenol and the fluorescence quenches 	Chemical	Janus sphere	[194]
Bio-materials	Neutrophil	Spore@Fe ₃ O ₄ @CDs	<ul style="list-style-type: none"> Encapsulation of metal oxides on spore surfaces through electrostatic interactions CDs loaded by chemical linker Urease loaded on the surface of neutrophils via the biotin system 	Magnetic	Droplet	[12]
		Neutrophil@Urease@Ag		Chemical	Microparticle	[195]

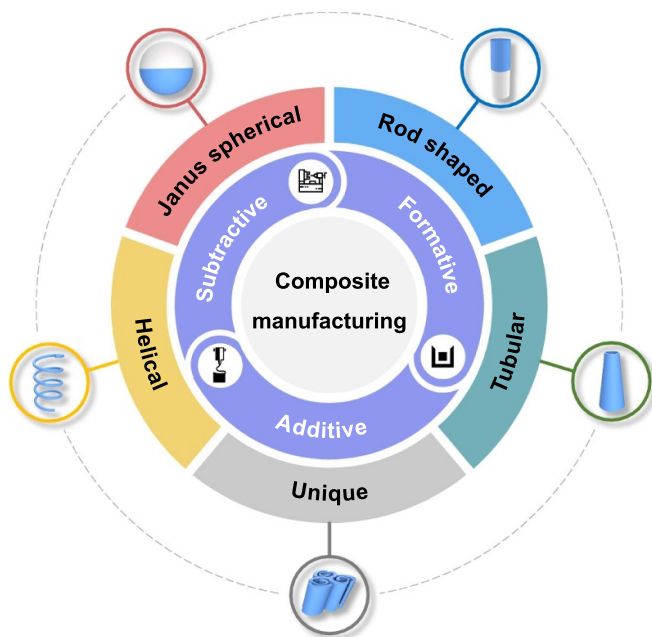


Figure 4. Composite manufacturing of each functional structure of MNRs.

3.2.1. MNRs based on volume divided Janus spheres. The Janus spheres, divided by volume, have distinct material compositions on both the surface and inside of their two hemispheres. Microfluidic synthesis offers a straightforward and cost-effective approach to creating these asymmetric structures without the need for a substrate. Moreover, Janus spherical MNRs of various sizes can be fabricated by adjusting the channel size, solution composition, and flow rate. Figure 6(a) shows the fabrication of multifunctional Janus spherical MNRs by microfluidic synthesis [253]. Various functions of MNRs can be achieved by adding functional NPs to the channel solution. For example, Pt NPs can be added to provide mobility, while Fe_3O_4 NPs can be added to improve controllability. It is important to note that the two hemispheres can be separated in a controlled manner by combining the phase separation method during the fabrication process. This results in the fabrication of a double spherical structure [254]. If further combined with WCE, the fabrication of spherical structures with depressions can be realized [255]. Moreover, the controllable tuning of double spherical and spherical structures with depressions can be realized by controlling the phase separation process [256].

In summary, microfluidic synthesis offers great potential for the fabrication of multifunctional Janus spherical MNRs. Moreover, the variety of shapes of volume divided Janus spheres can be extended by combining phase separation and WCE methods. However, the inability to control the distribution of functional NPs on the surface is still a major constraint in the fabrication of high performance MNRs. To prevent the mixing of different phases by convection, a low fluid flow rate is used, resulting in low flux problems. Therefore, advanced NPs arrangement control technology and high-throughput

fluid control technology have become the trend of microfluidic synthesis for the fabrication of Janus spherical MNRs.

3.2.2. MNRs based on surface divided Janus spheres.

Unlike volume divided Janus spheres, surface divided Janus spheres exhibit asymmetric material distribution only on the outer surface (figure 6). Moreover, in contrast to volume divided Janus spheres, which need to be doped with functional NPs to obtain functionality, surface divided Janus spheres incorporate functional materials into the substrate in the form of coatings. Although the substrate is required and to some extent less stable and reliable than the volume divided Janus spheres, the distribution of functional materials on the outer surface becomes controllable and uniform, which opens up opportunities for high performance MNRs.

PVD stands out as the most commonly employed coating technique for depositing functional materials onto substrates. Through the deposition of catalytic materials such as Pt [55], inert materials like Ti [189] (used to protect self-fuel such as Al), and magnetic materials like Ni [242] and Fe [146], MNRs can be endowed with mobility and controllability, respectively. In figure 6(b), the process of fabricating the multifunctional Janus spherical MNRs is illustrated, involving the continuous deposition of functional materials through PVD [257]. The Au coating serves the dual purpose of protecting Fe from oxidation and providing an affinity interface for subsequent functionalisation modifications. It is important to highlight that PVD is characterized by line-of-sight deposition, meaning that it cannot deposit functional materials on areas that are obscured. Consequently, Janus spheres produced through the PVD method typically feature a coating of functional material on only one half of the surface. In contrast, ALD, an alternative coating technique employing chemical vapor deposition (CVD), allows for the deposition on all sides of the spherical substrates exposed to the environment, except for the areas in contact with the bottom surface. As a result, Janus spheres obtained through ALD exhibit more than half-coated functional material. This presents an opportunity to extend the lifespan of Janus spherical MNRs, especially those propelled by consuming self-fuel (e.g. Mg, Al). Figure 6(c) illustrates Janus spherical MNRs fabricated through ALD, showcasing a more than half-coated configuration achieved by depositing TiO_2 (an inert material) onto Mg spherical substrates [258]. The large area of the inert material coating led to a significant reduction in the contact area of the Mg sphere substrate with the environment, resulting in a decreased rate of Mg depletion and an extended operational lifespan. Additionally, ALD is often synergistically employed with PVD due to its lower efficiency and operational complexity. While PVD is utilized for depositing functional materials, ALD is employed for depositing inert oxide materials such as TiO_2 [259] and Al_2O_3 [260].

In summary, PVD and ALD present an opportunity for the fabrication of multi-functional and high performance Janus spherical MNRs. Furthermore, the efficiency and versatility of surface-divided Janus spherical MNRs can be enhanced through the synergistic interplay of these two techniques.

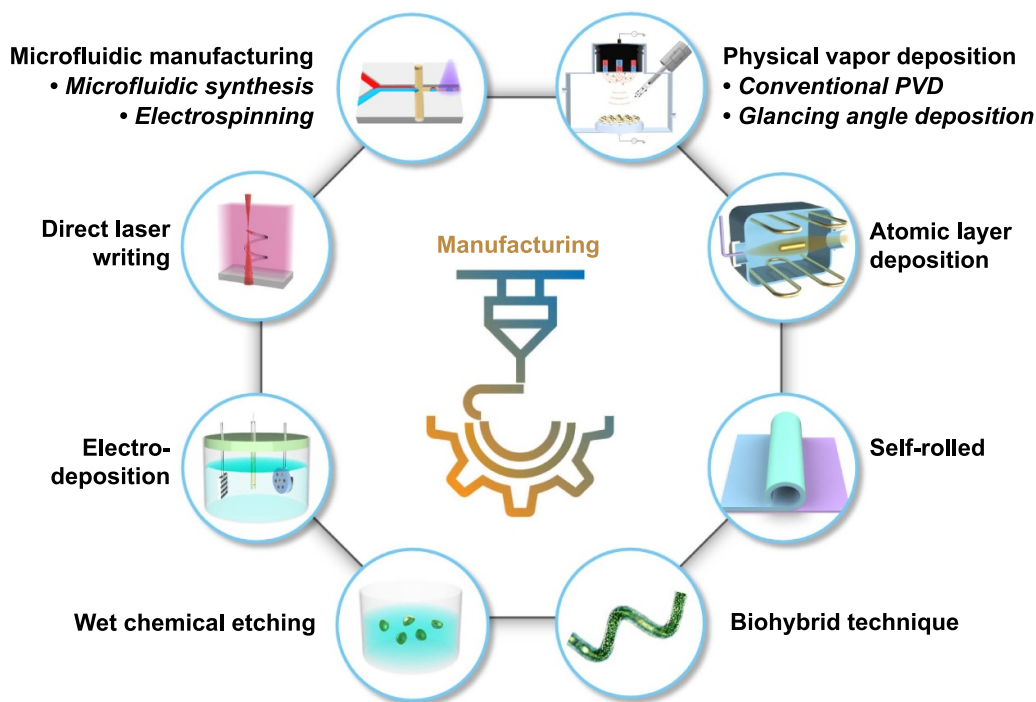


Figure 5. Various manufacturing methods for MNRs.

However, prior to utilizing PVD and ALD methods for Janus sphere fabrication, the spherical substrates need to undergo pre-treatment to ensure dense and monolayered assembly, thereby ensuring the quality and homogeneity of the coating. An effective solution is a composite manufacturing method that incorporates microfluidic synthesis. The microfluidic synthesis technique enables the attainment of uniform monolayer tiling of spherical substrates during the fabrication process, eliminating the need for post-processing. Therefore, exploring the composite manufacturing method combining PVD, ALD with microfluidic synthesis technique can enhance the fabrication efficiency of surface divided Janus spheres for MNRs.

3.3. Rod-shaped MNRs

In contrast to Janus spherical MNRs, non-spherical MNRs are susceptible to tumbling, twisting, and rotating in dynamic fluids, facilitating their contact and interaction with the environment. One typical application of this behavior is seen in thrombolysis [261]. Rods with an aspect ratio are typical of non-spherical shapes. Similar to Janus spheres, the asymmetry of these rods is achieved through the asymmetric distribution of materials. Depending on how the material is distributed, non-spherical MNRs can be categorized as radial multi-material rods and axial multi-material rods. Figure 7 depicts two types of rods along with their corresponding manufacturing techniques, as well as the procedures for acquiring functional materials.

3.3.1. MNRs based on radial multi-material rods. Radial multi-material rods exhibit variations in materials along the radial direction, often exemplified by Janus rods composed of two semi-cylinders. Similar to volume divided Janus spheres, microfluidic manufacturing techniques can be employed for the fabrication of radial multi-material rods. The distinctive aspect lies in the prevalent use of electrostatic spinning for the rapid production of rods. This method allows for the fabrication of rod-shaped MNRs with diverse diameters and material layouts by controlling parameters such as nozzle aperture and shape, voltage magnitude, solution concentration, and flow rate. Figure 7(a) illustrates the fabrication of radial multi-material rods through side-by-side electrostatic spinning [261]. Given that the fibers produced by electrostatic spinning are continuous, cryosection is employed in conjunction to tailor the aspect ratios of the rods. CaO_2 NPs are introduced by doping on one side of the rod-shaped MNRs to impart mobility. On the opposite side of the rod-shaped MNRs, the carboxylated interface of maleic anhydride modified-poly(lactic acid) creates an opportunity for subsequent loading of the drug Arg-Gly-Asp (RGD). The incorporation of SiPc material, also achieved through doping, generates reactive oxygen species for thrombolysis. Additionally, the unique shape of the radial multi-material rods allows the MNRs to use the column surface as the flow-facing surface, thereby increasing the likelihood of RGD-platelet interaction and consequently improving the thrombolytic performance of the MNRs.

In conclusion, electrostatic spinning stands out as a reliable choice for manufacturing multi-functional and high

Table 2. Overview of manufacturing methods for MNRs.

Type	Manufacturing method	Minimum feature size	Typical size range	Typical structures	Mass production	Typical materials	Advantages	Disadvantages
Additive manufacturing	Two dimensional Liquid phase deposition	>0.14 nm [229]	Thickness 5 nm–61 nm [65, 230]	Multilayer film Isotropic	√	PEM, PAH, PSS, CHI, ALG	<ul style="list-style-type: none"> • Easy • High precision • High controllability 	<ul style="list-style-type: none"> • Low efficiency
	Vapor phase deposition	>0.1 nm [231]	Thickness 2 nm–400 nm [55, 206]	Film ‘Line-of-sight’	×	Fe, Ni, Pt, Ti, Ag, Au, SiO ₂	<ul style="list-style-type: none"> • High efficiency • High purity 	<ul style="list-style-type: none"> • Poor step coverage • High equipment requirements
		Atomic layer deposition	>0.05 nm [232]	Thickness 7 nm–175 nm [115, 233]	Film Isotropic		Al ₂ O ₃ , ZnO, TiO ₂	<ul style="list-style-type: none"> • High precision • High uniformity • High step coverage
Three dimensional	Electrochemical methods	>10 nm [234]	Diameter 0.1 μm–5 μm [49, 235]	Rod/Tube/Helix		Fe, Ni, Pt, Ti, Ag, Au	<ul style="list-style-type: none"> • Low equipment requirements • High efficiency 	<ul style="list-style-type: none"> • Increased costs due to templates
	Photopolymerization methods	>13 nm [236]	Helix diameter 100 μm–900 μm [213] Sphere diameter 1.67 μm–500 μm [34, 237]	Janus sphere/Rod/Helix		PEDGA, CaCl ₂	<ul style="list-style-type: none"> • Excellent monodispersity • Easy modification 	<ul style="list-style-type: none"> • Low efficiency • Difficult to achieve nanoscale
Multi dimension		>600 nm [238]	0.012 mm–3 mm [239, 240]	Non-undercut structure	√	SU-8	<ul style="list-style-type: none"> • High resolution • Integration of components doable 	<ul style="list-style-type: none"> • Require clean room facilities and mask
		>18 nm [241]	2 μm–500 μm [242, 243]	Any shape	×	SU-8	<ul style="list-style-type: none"> • High resolution • 3D complex architectures are possible • Maskless • High biocompatibility • Versatility 	<ul style="list-style-type: none"> • Low efficiency • High equipment requirements • Complex • Security issues

(Continued.)

Table 2. (Continued.)

	Self-rolled	>1 μm [222]	Diameter 1 μm –500 μm [222, 244]	Tube/Helix	×	Fe, Ni, Pt, Ti, Ag, Au	• High material adaptability • Flexibility in design • Versatility • Easy • High yield	• Non-uniform size
Formative manufacturing	Phase separation	>53 nm [245]	0.145 μm – 100 μm [246, 247]	Janus sphere	√	TPM	• High yield • Low controllability • Low controllability • Low precision	• Not suitable for inorganic
Subtractive manufacturing	Wet chemical etching	>20 nm [248]	Ancillary manufacturing or Diameter 100 nm–700 nm [249, 250]	Any shape		Si, Ag, Cu, PS	• High yield • Low equipment requirements	• Low controllability • Low controllability • Low precision
	Dry etching	>8 nm [251]	Ancillary manufacturing 64 nm–4.5 μm [226, 252]	Any shape	×	Si, Au, CMS	• High resolution • High precision	• Low yield • High equipment requirements

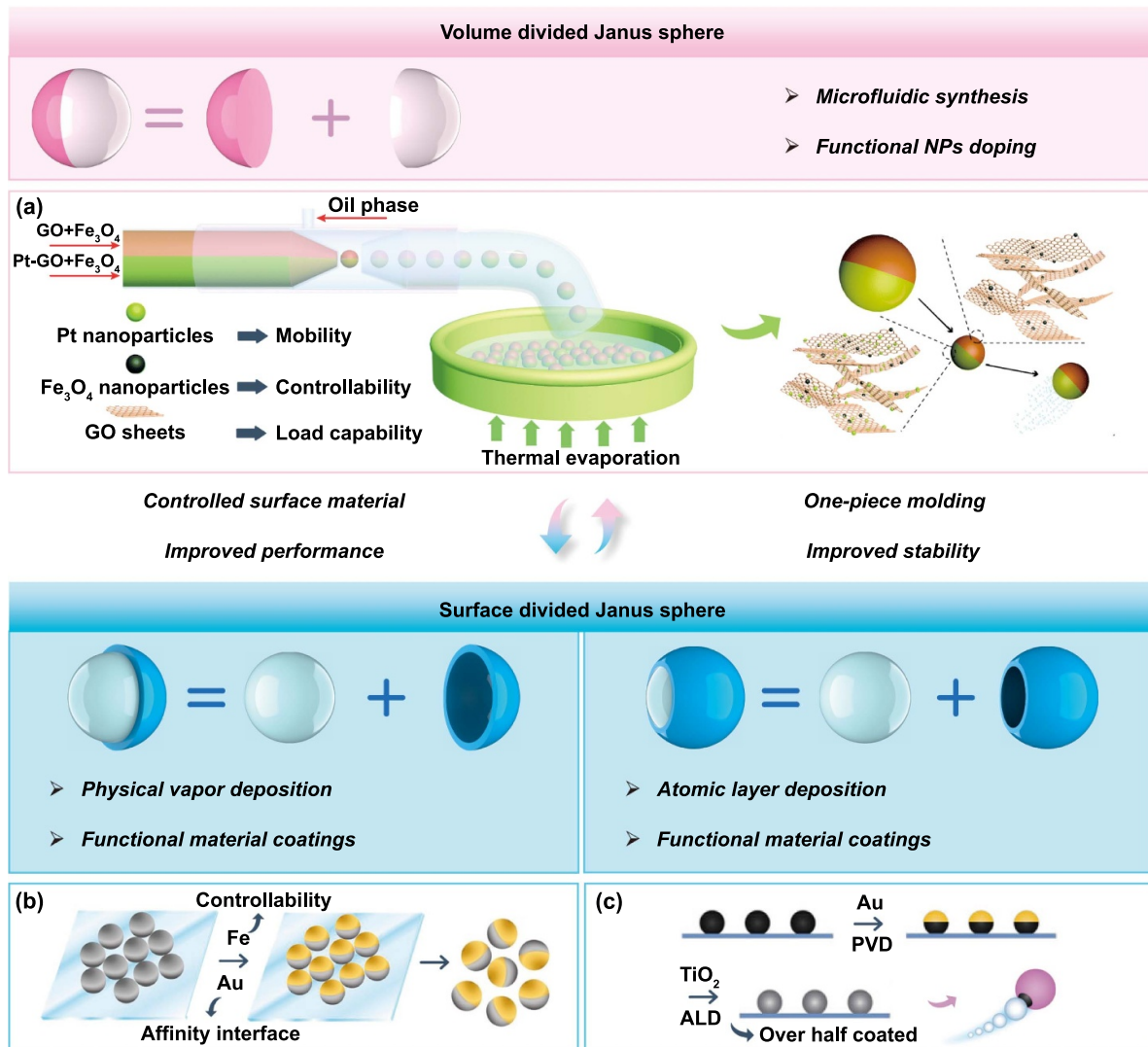


Figure 6. Composite manufacturing of Janus spherical MNRs. (a) Microfluidic synthetic fabricated volume divided Janus spheres. Adapted from [253] with permission from the Royal Society of Chemistry. (b) PVD fabricated surface divided Janus spheres. Reprinted (adapted) with permission from [257]. Copyright (2017) American Chemical Society. (c) ALD and PVD fabricated surface divided Janus spheres to grow MNRs lifetimes [258]. John Wiley & Sons. © 2021 Wiley-VCH GmbH.

performance rod-shaped MNRs. Furthermore, the production of rod-shaped MNRs with customized aspect ratios is attainable through collaboration with cryosection technology. However, challenges such as limitations in charge mobility and solubility persist in the fabrication of inorganic rods using electrostatic spinning. Consequently, the pursuit of inorganic materials compatible with electrostatic spinning and advancements in electrostatic spinning processes has emerged as a current trend in the fabrication of radial multi-material rods through electrostatic spinning.

3.3.2. MNRs based on axial multi-material rods. Unlike radial multi-material rods, axial multi-material rods feature multiple materials arranged in the axial direction. Furthermore, in contrast to radial multi-material rods fabricated through electrostatic spinning, where functionality is achieved by doping functional NPs, axial multi-material rods

integrate multiple functional materials through LbL deposition. Additionally, axial multi-material rods use the end face as the flow-facing surface, unlike radial multi-material rod-shaped MNRs, which use the cylindrical surface for this purpose. This design choice enhances the kinematic performance of high-aspect-ratio rod-shaped MNRs by minimizing drag forces, albeit at the potential cost of a slight reduction in the likelihood of the robot interacting with its target.

Template-assisted TAE stands out as the most common method for fabricating axial multi-material rods. In contrast to electrostatic spinning, which requires the combination with cryosection technology to control the aspect ratio of the rods, TAE achieves aspect ratio control by adjusting the applied charge and selecting membrane templates with different aperture sizes. Additionally, the fabrication of flexible rods becomes feasible by depositing flexible materials such as polypyrrole [6, 74]. Furthermore, the flexibility of rods can also be attained through a combination with WCE. Figure 7(b)

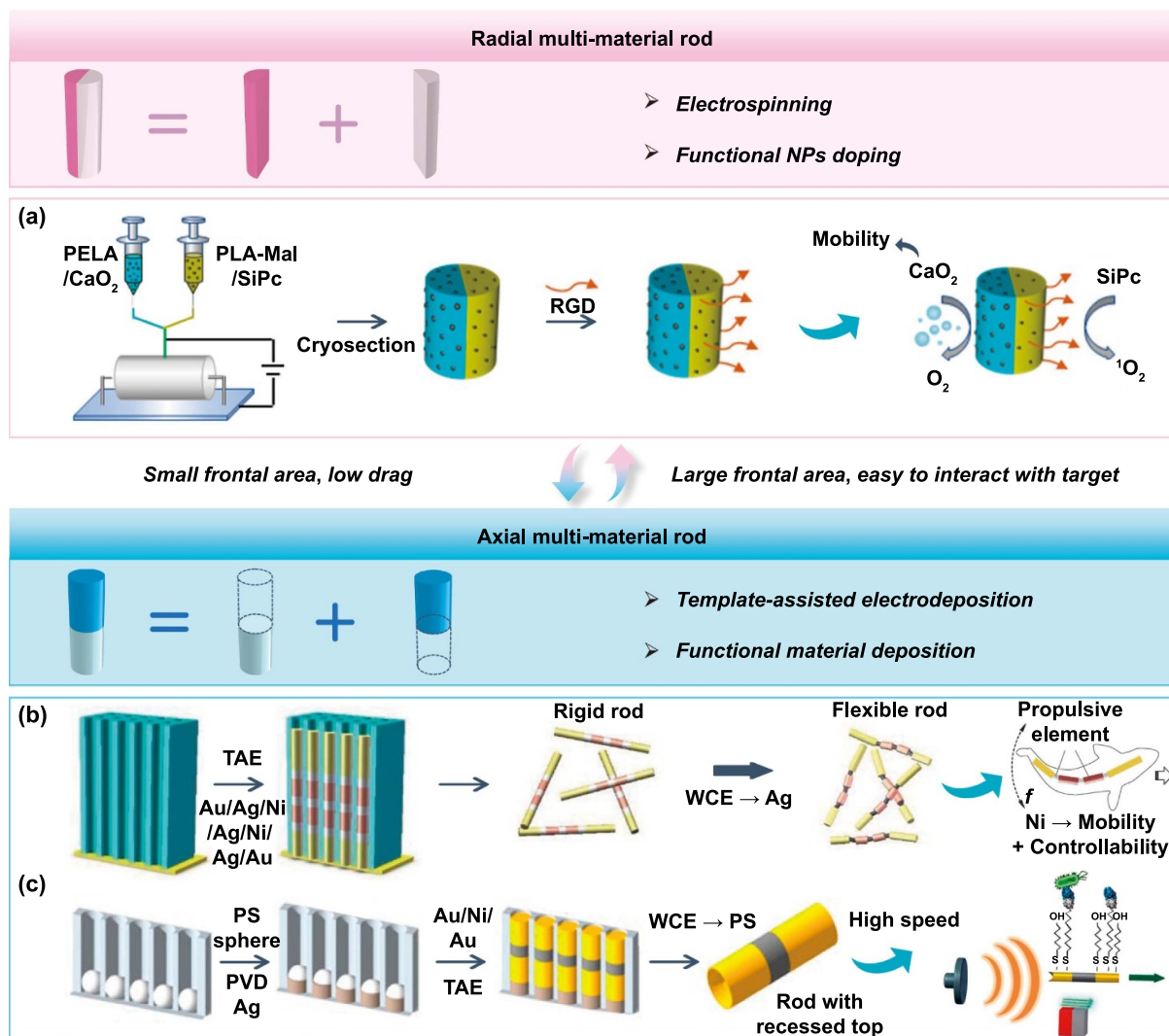


Figure 7. Composite manufacturing of rod-shaped MNRs. (a) Microfluidic synthesis to fabricate radially multi-material rod-like MNRs doped with functional NPs. Reprinted (adapted) with permission from [261]. Copyright (2021) American Chemical Society. (b) TAE combines WCE to fabricate flexible rod-shaped MNRs [169]. John Wiley & Sons. © 2016 WILEY-VCH Verlag GmbH & Co. KGaA, Weinheim. (c) TAE combines with WCE to fabricate rod-shaped MNRs that can be driven by ultrasound. Reprinted (adapted) with permission from [72]. Copyright (2013) American Chemical Society.

depicts the fabrication of radial multi-material rigid rods using TAE, coupled with WCE to produce flexible rods [169]. In this case, Ag segments are deposited to create flexible rods. The exciting flexibility of the Ag segments, partially corroded by WCE, adds to the overall appeal. Leveraging this flexible property along with the magnetic responsiveness of the Ni segment, the resulting flexible rod-shaped MNR exhibits a remarkable traveling wave motion when subjected to an oscillating magnetic field, akin to the graceful movement of a fish. In addition, the combination of TAE with WCE allows for the fabrication of rod-shaped MNRs featuring a depression at one end, capable of rapid propulsion under ultrasound stimulation. Figure 7(c) illustrates the process of fabricating such a rod-shaped MNR using TAE in conjunction with WCE [72]. In this method, PS spheres infiltrate the membrane template, providing an opportunity for subsequent etching to form a depression in the rod. Simultaneously, Au and Ni segments are introduced

to furnish an affinity interface and magnetic responsiveness for the MNR, facilitating subsequent functionalization and magnetic guidance. Furthermore, some researchers have explored the combination of TAE with LbL self-assembly and WCE to create hollow hinges [262].

In summary, the integration of TAE and WCE exhibits significant potential for the fabrication of axial multi-material rod-shaped MNRs. Particularly noteworthy are the resulting flexible rods and rods with one end recessed, which considerably enhance the kinematic performance of rod-shaped MNRs. However, TAE has limited material compatibility and typically cannot deposit non-conductive materials such as insulators and most non-metallic materials. CVD offers an effective solution to this limitation. CVD enables the deposition of non-conductive materials into the pores of the membrane template, allowing for the fabrication of non-conductive segments. Therefore, the composite manufacturing method combining

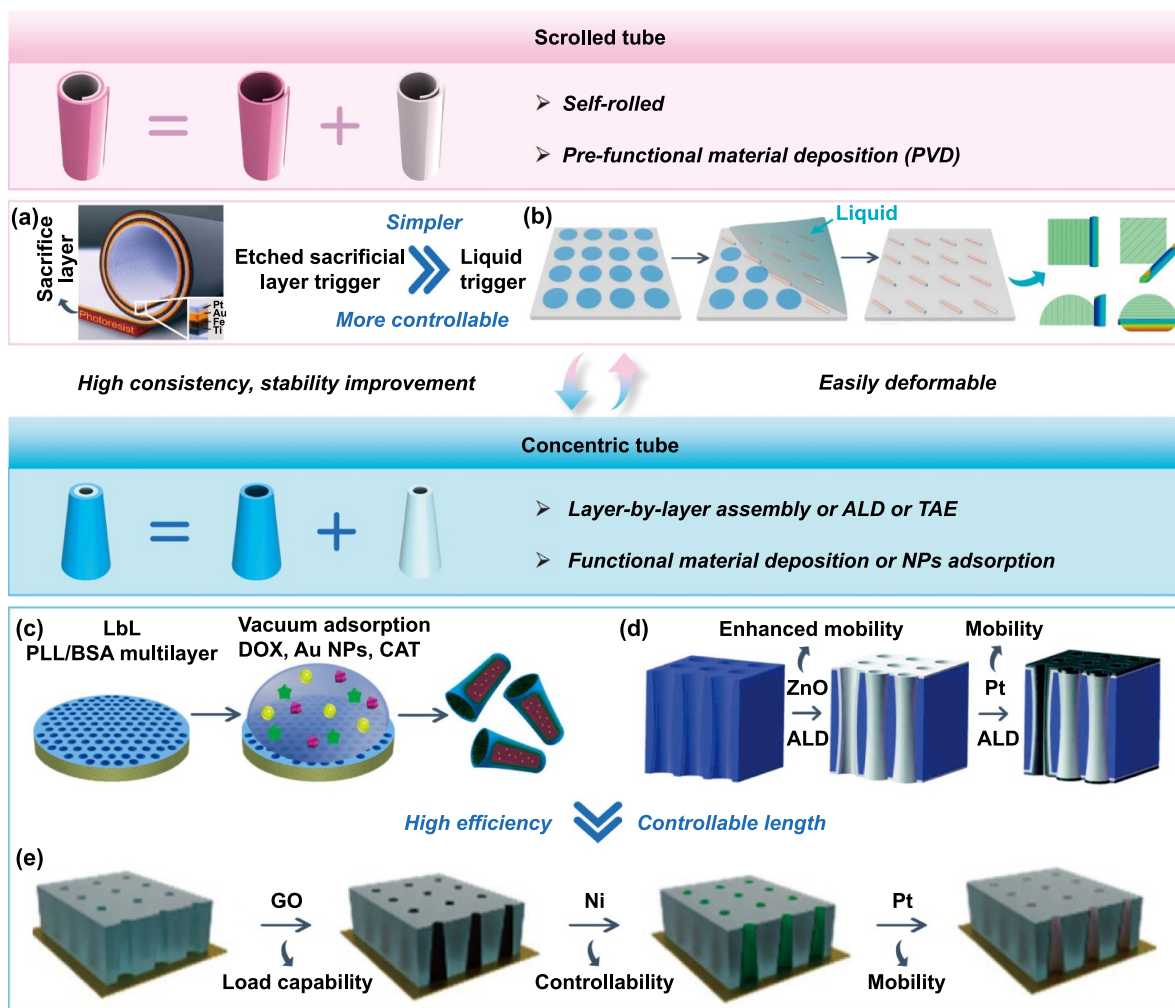


Figure 8. Composite manufacturing of tubular MNRs. (a) Sacrificial layer based self-rolled fabricated multifunctional scrolled tube [266]. John Wiley & Sons. Copyright © 2009 Wiley-VCH Verlag GmbH & Co. KGaA, Weinheim. (b) Droplet-triggered self-rolled to fabricate scrolled tubes. Reproduced from [267]. CC BY 4.0. (c) Fabrication of concentric tubes using the LbL self-assembly method. Reprinted (adapted) with permission from [148]. Copyright (2015) American Chemical Society. (d) With the help of polycarbonate templates, ALD manufactures multifunctional concentric tubes. Adapted from [269] with permission from the Royal Society of Chemistry. (e) TAE manufactures multifunctional concentric tubes with controllable lengths. Reproduced from [138]. CC BY 4.0.

TAE, WCE and CVD will enrich the material system of axial multi-material rod-shaped MNRs and provide wider opportunities for their multifunctionality and high performance.

3.4. Tubular MNRs

Compared to Janus spheres and rods, tubes stand out as the preferred structure for bubble-driven MNRs, primarily due to their internal space that facilitates the efficient generation and release of bubbles. In contrast to rods, where multiple materials are arranged along the radial or axial direction, the asymmetry of tubes arises from the different materials on their inner and outer surfaces. Tubes can be further categorized into scrolled tube and concentric tube based on the distribution of materials. Figure 8 provides an illustration of these two tube types and their manufacturing methods, as well as the methods of obtaining functional materials.

3.4.1. MNRs based on scrolled tubes. Scrolled tubes are created by rolling a thin film of functional material. While this rolling may reduce the structural shape stability of the scrolled tube, it introduces the possibility for intelligent deformation [263, 264]. Self-rolled is a prevalent technique for manufacturing scrolled tubes, leveraging the release of internal stresses within the functional thin film material. Consequently, the functional material film forms the basis for this fabrication method. The most commonly employed technique for producing functional material films is PVD. PVD allows the deposition of various functional materials onto the substrate. For tubular MNRs propelled by bubbles resulting from chemical reactions, the final layer of functional material is typically catalytic or self-fuel [222, 265]. It is important to note that there are two commonly employed methods for inducing stress release in thin films of functional materials. One approach involves depositing a material with internal stress onto a patterned photoresist and then releasing the stress in the film

by removing the sacrificial photoresist layer through WCE. Figure 8(a) illustrates the induced self-rolled through etching the sacrificial layer [266]. In this case, the innermost layer of the scrolled tube, Pt, contributes to its mobility. Compared to the method of etching the sacrificial layer, another method induced by liquid is simpler and more controllable. As WCE is isotropic, the liquid-induced method allows the controlled preparation of scrolled tubes with different curl directions by controlling the contact point of the liquid. Figure 8(b) shows the liquid-induced self-rolled and demonstrates the robust controllability of the method [267].

In conclusion, the combination of self-rolled, PVD, and WCE presents a convenient approach for crafting scrolled tubular MNRs with adjustable diameters and lengths. The geometry of the scrolled tubes can be effectively controlled through a nuanced understanding of micro- and nano-scale mechanics and meticulous tuning of deposition parameters. However, challenges such as the inhomogeneous thickness and poor uniformity of the tubes must be overcome. Consequently, there is a growing trend towards the development of advanced self-rolled process control techniques to enhance the fabrication of scrolled tubes.

3.4.2. MNRs based on concentric tubes. Unlike scrolled tubes, concentric tubes are seamless structures with multiple materials arranged in concentric layers, resulting in higher structural stability. Various manufacturing methods for concentric tubes often involve membrane templates, including LbL self-assembly, ALD, and TAE. In LbL self-assembly, polymeric materials with oppositely charged surfaces are deposited into the interior of holes in the membrane [66, 148, 181, 268]. The charged surface of the polymer enables the loading of various functional NPs or cargoes, through non-covalent interactions like electrostatic interactions. In contrast to LbL self-assembly, ALD manufactures concentric tubular MNRs by directly depositing functional materials into the pores on the membrane [269]. Figures 8(c) and (d) depict the fabrication of multifunctional and high performance concentric tubes for MNRs using LbL self-assembly and ALD, respectively [148, 269]. However, since both methods involve deposition to fill the entire hole in the membrane, LbL self-assembly and ALD lack control over the length of the concentric tubes, which is constrained by the thickness of the membrane. In contrast, TAE proves to be an ideal method for crafting concentric tubes with controllable length. Furthermore, its fabrication efficiency is enhanced due to electrical energy input. Unlike the TAE method for axial deposition in fabricated rods, radial deposition in fabricated tubes can be achieved by adjusting parameters such as current density and current direction. Additionally, the length of the tube can be precisely controlled by controlling the deposition time. Figure 8(e) illustrates the process of fabricating a multifunctional concentric tubular MNRs using the TAE method [138].

In summary, LbL self-assembly, ALD, and TAE offer promising avenues for the fabrication of multifunctional and high performance concentric tubular MNRs. Notably, the TAE

method stands out for its unique ability to control the length-to-diameter ratio of the concentric tubes. However, it is important to note that all of these methods rely on membrane templates, which potentially increases the cost of fabrication.

3.5. Helical MNRs

In contrast to Janus spheres, rods, and tubes, the helix is inherently chiral, imparting asymmetry to its structure. Rotational motion along the helix axis enables axial translational motion. Therefore, helices are commonly employed as structures for magnetically driven MNRs. Depending on the method of obtaining the helix, it can be categorized as a biological helix or an artificial helix. Figure 9 illustrates the two types of helical MNRs and their corresponding manufacturing techniques, as well as the procedures for acquiring functional materials.

3.5.1. Biological helical MNRs. Biological helices are directly obtained from the natural environment, rendering them highly biocompatible. The biotemplate synthesis method, particularly based on helical plant vessels, offers a simple, low-cost, and large-scale approach for fabricating magnetic helical MNRs. Figure 9(a) depicts the magnetic plant helical MNRs fabrication process [270]. The Ti layer serves as an external biocompatible coating to mitigate potential toxicity associated with the Ni layer. Additionally, the helix diameter and pitch can be adjusted through mechanical stretching; however, the use of photoresist is necessary to fix the shape. In comparison, *Spirulina* possesses a naturally intact helical structure, obviating the need for a series of post-processing operations. Additionally, *Spirulina* exhibits properties such as degradability and autofluorescence. Leveraging its biosurface affinity, functional NPs can be easily loaded. Figure 9(b) illustrates a straightforward, cost-effective, and scalable fabrication method for helical MNRs designed for drug delivery, utilizing *Spirulina* [271]. Superparamagnetic NPs are adsorbed on the surface of MNRs, allowing them to perform controlled motions under magnetic fields. Furthermore, the inherent properties of *Spirulina* allow the MNR to conduct fluorescence imaging *in vivo* without requiring any surface modification. Additionally, studies have reported that parameters such as helicity and helix diameter of the helix can be adjusted by manipulating the living environment of the natural helix [272]. Furthermore, with the application of annealing treatment, hollow helix structures can be created by removing helix core [272].

In summary, the use of biological helices offers a straightforward approach for the batch fabrication of helical MNRs. Furthermore, when combined with PVD or the adsorption of magnetic NPs, magnetic MNRs with high biocompatibility can be easily produced. However, natural helical biotemplates from the environment are evidently insufficient to meet the demands for helical structures in MNRs within increasingly complex application scenarios. Particularly, the tuning of biotemplates is currently restricted to the overall structural parameters of the helix and rarely involves adjustments to

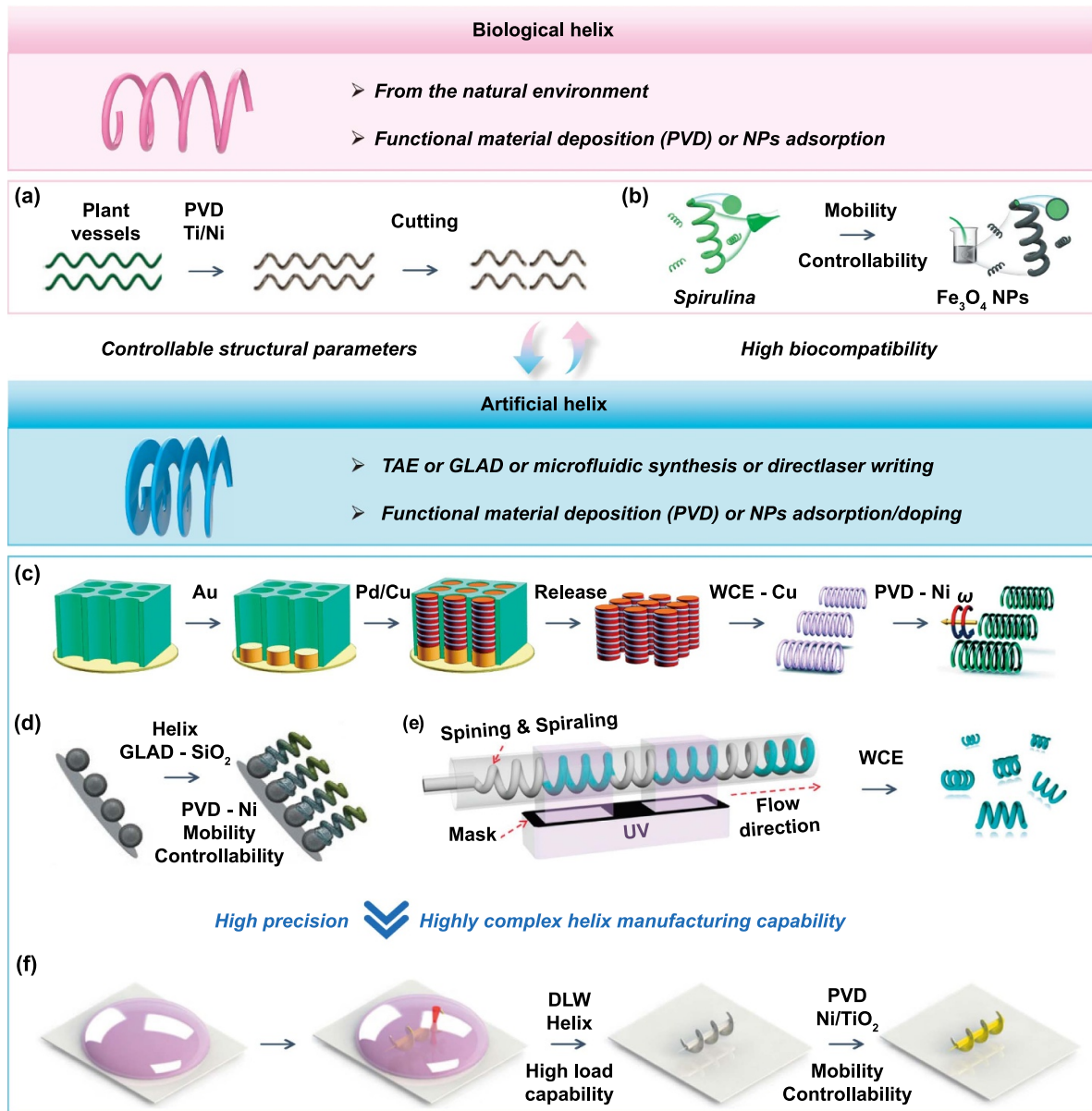


Figure 9. Composite manufacturing of helical MNRs. (a) Manufacturing process of the plant-based magnetic spiral microrobots. Reprinted (adapted) with permission from [270]. Copyright (Year) American Chemical Society. (b) Helical MNRs based on Spirulina. Reprinted from [271], © 2024 Elsevier B.V. All rights reserved. (c) TAE combines WCE and PVD to fabricate multifunctional helices. Adapted from [227] with permission from the Royal Society of Chemistry. (d) GLAD combined with PVD manufacture magnetic helices. From [274]. Reprinted with permission from AAAS. (e) Microfluidic synthesis combined with WCE to fabricate polymer helices [276]. John Wiley & Sons. © 2017 Wiley-VCH Verlag GmbH & Co. KGaA, Weinheim (f) DLW combined with PVD to manufactures magnetic needle-type helix with complex mesh structures [173]. John Wiley & Sons. © 2020 WILEY-VCH Verlag GmbH & Co. KGaA, Weinheim.

the wire diameter. Hence, the development of more controllable biological helices represents a key research direction for helical MNRs.

3.5.2. Artificial helical MNRs. Unlike biological helices, artificial helices are helical structures that are artificially created or synthesized. Compared to biological helices, the structural parameters of artificial helices are more controllable. Moreover, the complexity of the helical structure can be made

higher, for example, double helix structure [56, 273]. There are many methods to fabricate helices, such as TAE, glancing angle deposition (GLAD), microfluidic synthesis, and DLW. The fabrication of helices using TAE involves a combination of WCE and PVD. In figure 9(c), the fabrication process of helices using TAE is illustrated [227]. Following the co-deposition of Cu and Pd, the Pd helical structure is obtained by selectively removing Cu through WCE, and the multifunctional material coating is applied via PVD. Furthermore, the fabrication of Pd helices with different aspect ratios can be

achieved by adjusting the applied charge, selecting templates with varying pore sizes, and modifying the solution composition. However, only the existence of helical co-deposition process of Cu and Pd has been found, which limits the wide application of this method. In comparison, GLAD facilitates the fabrication of a more diverse array of helical structures using a broader range of applicable materials. Essentially, GLAD is a variant of PVD in which the substrate changes from being perpendicular to the incident vapor flux to having a certain bevel angle, and the substrate shifts from static to rotating. By adjusting the bevel angle size and the rotation speed during the deposition process, the parameters of the helical structure can be controlled. Figure 9(d) illustrates the process of manufacturing helices using GLAD [274]. It is noteworthy that the materials required for each function can be directly obtained through the GLAD method, or functional materials can be deposited after adjusting the bevel angle to PVD mode. This multi-process composite *in-situ* molding technique provides an opportunity for the automated and highly reliable fabrication of multifunctional and high performance helical MNRs. However, GLAD requires seeds as the starting point for helix generation, and these seeds must be densely arranged and monolayered. Typically, seeds are spherical particles, and the combination of dry etching can further reduce the seed size, thus offering the possibility of obtaining smaller helices [275]. In comparison, microfluidic synthesis is a direct molding process that eliminates the need for seeds. Figure 9(e) illustrates the fabrication of multifunctional helical MNRs using microfluidic synthesis [276]. This method leverages gelation and the unbalanced friction of gel microfibers with the surrounding fluid to form helical structures. It involves selective curing of the helices through discrete UV illumination and the subsequent removal of uncured regions via WCE to obtain the helices. By controlling the flow rate of the fluid and the frequency of UV illumination, highly controllable helical lengths, pitches, and diameters can be achieved. Furthermore, Janus helix, hollow helix, and core-shell helical MNRs can be realized by altering the number and structure of the flow channels [276]. The multifunctionality of these structures is achieved through the doping of functional NPs. Compared to the aforementioned fabrication methods, DLW, thanks to its high precision and customizability, can manufacture helices with more intricate structures, including double helices [71] and helices with microstructures [277]. In figure 9(f), the fabrication of needle-type helix with mesh structure using DLW is demonstrated [173]. Their multifunctional properties can be realized by various methods, such as coating of functional materials by PVD, adsorption or doping with functional NPs doping.

In summary, various methods, including TAE, GLAD, microfluidic synthesis, and DLW, can be employed for the fabrication of helical MNRs. Furthermore, by integrating the PVD method, multifunctional helical MNRs can be conveniently obtained. Particularly, the DLW method, with its enhanced 3D structure fabrication capability, can produce helical MNRs with intricate microstructures, significantly enhancing their performance. However, the point-by-point printing approach of DLW restricts its ability to mass-produce helices.

Hence, advancements in DLW manufacturing processes are crucial for enhancing the versatility and performance of helical MNRs.

3.6. MNRs with unique structures

In addition to the structures mentioned above, there are still several unique structures for MNRs. Benefiting from their properties, these structures provide a viable solution for MNRs to move towards high performance. Based on the dimensionality of these structures, they can be categorized as 3D unique structures, shell structures, and surface microstructures. Figure 10 illustrates these three unique structures and their corresponding manufacturing techniques, as well as the procedures for acquiring functional materials.

3.6.1. MNRs with 3D unique structures. 3D unique structures bring special structural properties that can bring the possibility of enhancing the performance of MNRs, especially the kinematic performance. Taking advantage of the powerful 3D structure customization capability of DLW, structures that can significantly increase the speed of optical, chemical, and ultrasonic driven MNRs have been fabricated. Figure 10(a) shows the fabrication process of a unique cavity structure for enhancing the velocity of ultrasonically driven MNRs using DLW [215]. The cavity was fabricated with a double fold-back microstructure, which increased the repulsion of the fluid and improves the stability of the bubbles. This work was the first to achieve effective propulsion at high shear rates in complex biofluids. In addition, the 3D structure of multiple nozzles and the interface enhancement properties of the sawtooth-like structure with multiple channels and nanointerfaces were utilized to significantly improve the kinematic performance of the optically and chemically driven MNRs, respectively [278, 279]. Moreover, the remarkable structures found in nature offer new avenues for high performance MNRs. Figure 10(b) depicts the transformation of sunflower pollen into intelligent urchin-like MNRs through WCE, PVD, and vacuum loading processes [280]. The huge internal cavity structure of sunflower pollen provides it with a robust cargo loading capability, while the ordered spikes on its surface facilitate efficient cell penetration.

3.6.2. MNRs with shell structures. Shell structures as asymmetric pseudo 3D structures can also contribute to the performance enhancement of MNRs. The combination of PVD and WCE is a typical method for manufacturing shell structures. Figure 10(c) shows the fabrication process of catalytic shell-structured MNRs using this method [206]. Pt, Ag, and Au were sequentially deposited on a silicon sphere by the PVD method. The innermost layer (Pt layer) served as a catalyst layer to provide mobility, the middle layer (Ag layer) acted as a support structure, and the outermost layer (Au layer) served as a protective layer. The silicon spheres were then etched using hydrofluoric acid to fabricate shell-structured MNRs. Moreover, the fabrication of 2 μm –30 μm shell-structured

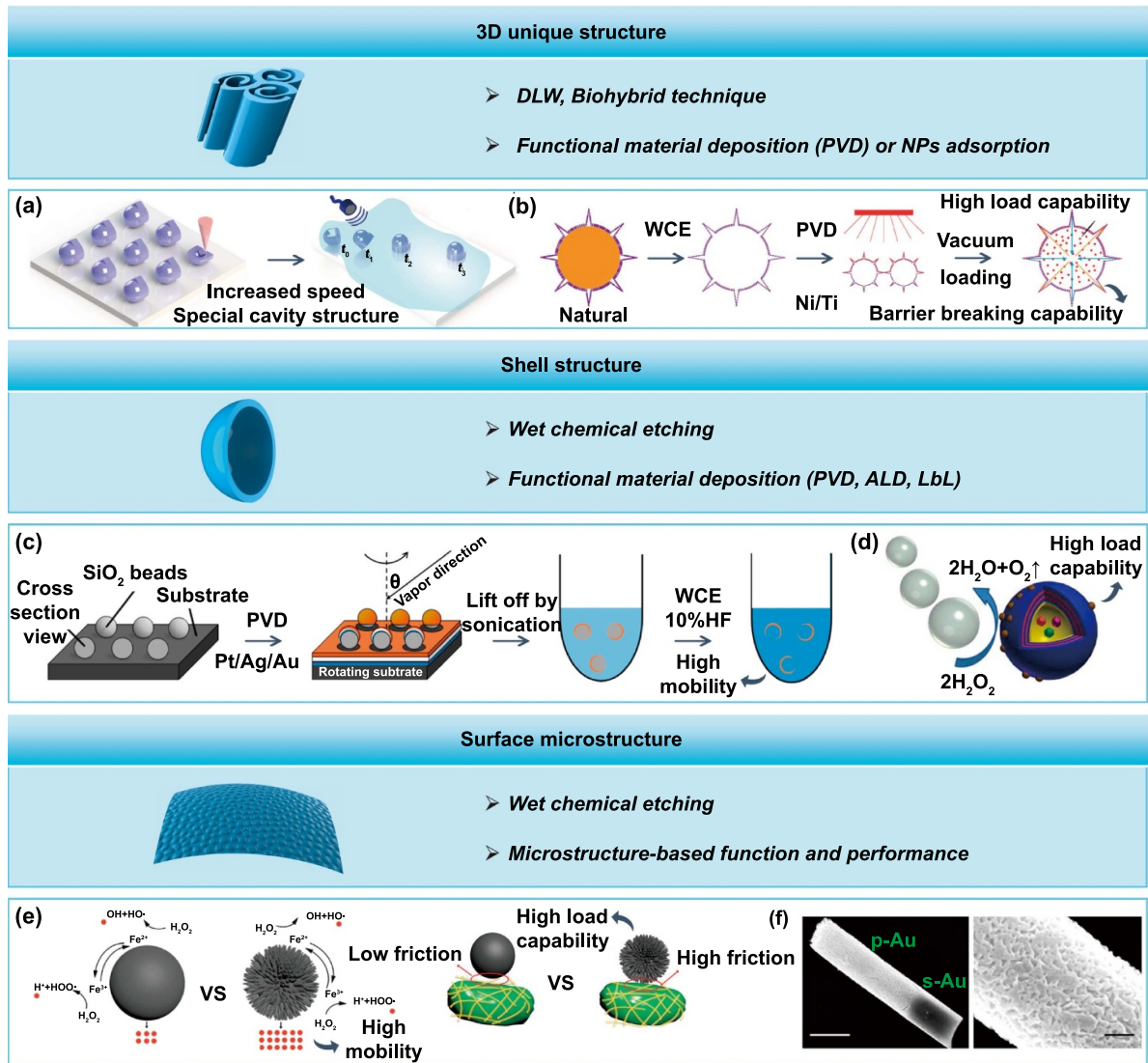


Figure 10. Composite manufacturing of MNRs with unique structure. (a) DLW fabricates ultrasound-driven MNRs with cavity structures. Reproduced from [215]. CC BY 4.0. (b) Biohybridization combined with WCE and PVD for the fabrication of smart urchin-like MNRs [280]. John Wiley & Sons. © 2020 WILEY-VCH Verlag GmbH & Co. KGaA, Weinheim. (c) PVD combined with WCE to fabricate bubble-driven hemispherical shell-shaped MNRs. Reprinted (adapted) with permission from [206]. Copyright (2014) American Chemical Society. (d) Hollow spherical structure with strong cargo loading capability. Reprinted (adapted) with permission from [205]. Copyright (2012) American Chemical Society. (e) High performance spherical MNRs fabricated by full-surface etching. Reprinted (adapted) with permission from [281]. Copyright (2021) American Chemical Society. (f) Selective surface etching to fabricate microstructures for enhanced MNR mobility. Reprinted (adapted) with permission from [282]. Copyright (2015) American Chemical Society.

MNRs can be fabricated by changing the diameter of the silicon spheres. The catalytic effect of this concave surface can give the MNR a stronger kinematic performance compared to the convex surface of the Janus sphere of the same size as a catalytic surface, due to its greater tendency to generate bubbles. In addition, this shell-structured microrobot can be driven by ultrasound and exhibit efficient cargo transportation capability [64]. In addition to hemispherical shell structures, overall spherical shell structures also exhibit strong cargo loading and transportation capabilities. Figure 10(d) shows the MNR for the overall spherical shell structure [205]. Using SiO₂ microspheres as templates, LbL self-assembly was

used to fabricate multilayer polymer films. Microcontact printing was used to asymmetrically endow the films with functional NPs. WCE was used to remove the templates. Finally, the MNRs were formed as overall spherical shell structures with strong cargo delivery capabilities as well as controllable encapsulation and triggered release capabilities.

3.6.3. MNRs with surface microstructures. The rational use of surface microstructures can significantly enhance the performance of MNRs. The most commonly used method for fabricating surface microstructures is WCE. There are two

ways to fabricate surface microstructures by WCE method, one is isotropic full-surface etching and the other is selective etching. Figure 10(e) shows the Fe_3O_4 microparticles (MPs) exhibit outstanding properties after the full-surface etching [281]. The Fe_3O_4 MPs have higher specific surface area and more active sites after the full-surface etching, giving them enhanced mobility and loading capability. Figure 10(f) shows an MNR with surface microstructure fabricated by combining TAE and WCE [282]. The use of microstructures gives it a stronger loading capability, which carries more lysozyme and enhances the bactericidal ability.

In summary, the powerful 3D structure fabrication capability of DLW and the powerful structure modification capability of WCE create a huge development space for the fabrication of multifunctional and high performance MNRs with complex structures. The application of unique structures also paves the way for the improvement of the performance of MNRs. However, with the increase of structural complexity, the non-selective or isotropic way of functional material conferment restricts the further development of high performance MNRs with multifunctional and complex structures. Therefore, the development of more selective and controllable functional material implantation methods is an important development area for the future fabrication of high performance MNRs.

3.7 Summary

Taking advantage of the diverse combinations, the AFS-CM method can be adapted to the fabrication of MNRs with different applications. Therefore, the AFS-CM method has become a mainstream manufacturing solution for MNRs. Currently, the research of smart materials applied to MNRs has become a major hotspot. The utilization of these materials enables the automation and intelligent control of MNRs in specific environments. For example, the light-responsive isomerization of azobenzene to remotely control the disassembly and assembly of the main body and functional components of the nanorobot [69], the spiropyran to control the start and stop of the nanorobot [70], and other pH-responsive or thermo-responsive hydrogels [186, 283, 284]. However, the current fabrication methods for MNRs using smart materials are still in the development stage. Therefore, exploring more diverse fabrication methods that can incorporate smart materials will be an important driving force for the development of smart and high performance MNRs.

In addition, as shown in the previous section, PVD deposition of functional materials, and doping and adsorption of functional NPs are important ways to confer multifunctionality to MNRs. However, functional NPs doping can limit the minimum feature size for fabrication, and the long-time reliability of functional NPs adsorption in complex environments is still debatable. Therefore, PVD has become the dominant functionality-conferring technology nowadays. In addition, the strong capability of DLW in fabricating complex 3D structures makes it an important fabrication method for manufacturing the bodies of MNRs. However, the current composite fabrication process of PVD and DLW is still relatively homogeneous, which only utilizes PVD to deposit

functional materials after DLW fabrication. Exploring more composite fabrication processes of the two may bring transformative breakthroughs to multifunctional and high performance MNRs. In addition, the current way to fabricate surface microstructures mostly uses WCE, but this does not allow for precise control of the microstructure. In contrast, the self-rolled method may provide feasibility for customized microstructures [285]. Therefore, exploring the process of controllable fabrication of surface microstructures for MNRs by the self-rolled method could bring great potential to high performance MNRs.

4. Discussion and future trends

4.1 Discussion

The coupled design and AFS-CM methods contribute to the development of high performance MNRs, which are expected to play an important role in a variety of potential applications such as biomedicine, environmental remediation, and micro- and nanomanufacturing. For the coupled design methods of high performance MNRs, we have explored three aspects: material-function integrated design, interface-performance integrated design, and structure-performance integrated design. Notably, there is an increasing interest in the design of surface microstructures of MNRs. For example, designing microstructures on the surfaces of MNRs driven by catalytic reactions can enhance the catalytic efficiency and hence the motional performance of MNRs. In addition, existing manufacturing methods are summarized and the use of AFS-CM methods to achieve highly integrated manufacturing of functional structures of MNRs is discussed in detail. DLW has received focused attention from researchers because of its unique advantages in manufacturing complex 3D structures at the micro- and nanoscale. Although a variety of future MNRs have been proposed, their design and manufacturing still face a number of challenges.

An ideal design of high performance MNRs should be a multi-factor coupled design that integrates functional requirements, application environment characteristics and materials/structures/processes. However, most of the existing designs are subjective. Moreover, due to different knowledge systems, researchers have different design ideas, which leads to difficulties in achieving optimal design when dealing with such multi-factor coupled problems. Therefore, it is necessary to develop an intelligent design system. It has the ability to independently design the materials/interfaces/structures/processes of MNRs according to different application requirements, and can rationally weigh and evaluate multiple factors to achieve the goal of multifunctional compatibility and optimal overall performance of MNRs. Meanwhile, on this basis, scientific design specifications and protocols for MNRs can be formed, thus promoting the development and commercialization of MNRs. In terms of manufacturing, the ideal manufacturing method of MNRs should be high-precision, high-efficiency, low-cost and scalable. However, existing composite manufacturing methods still have shortcomings in terms of manufacturing efficiency, manufacturing risk, and manufacturing

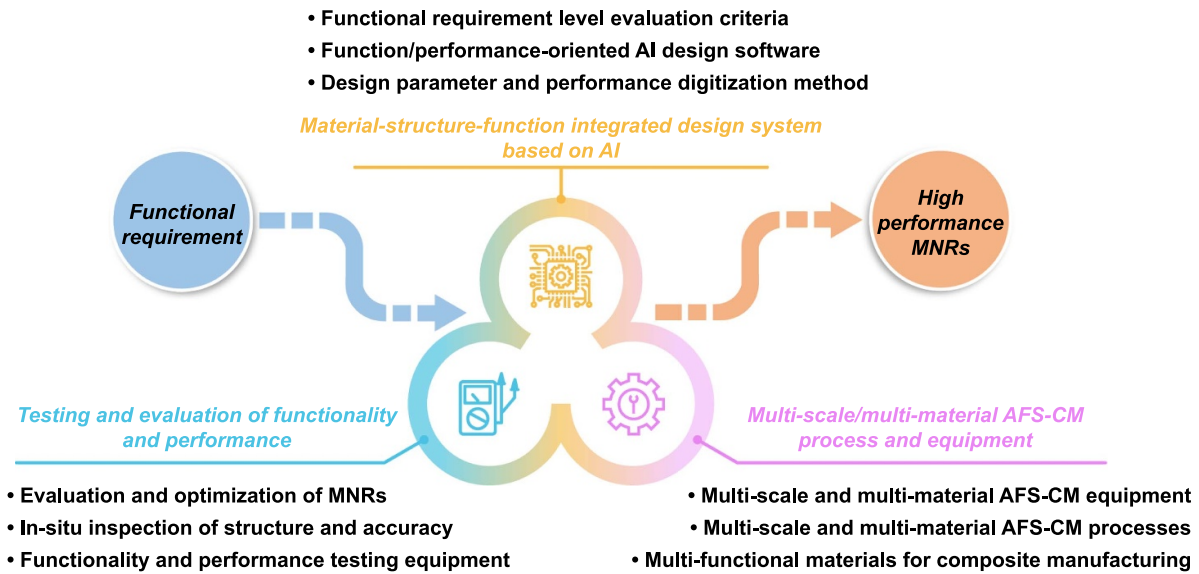


Figure 11. Trends in design, manufacturing and testing of high performance MNRs.

cost, such as the composite of multiple manufacturing processes increases the complexity of manufacturing, the step-by-step nature increases the risk of failure, and the demand for multi-material/multi-scale increases the manufacturing cost. Therefore, it is important to develop new integrated manufacturing processes and equipment that combine the advantages of additive, formative and subtractive manufacturing methods.

4.2. Future trends

As an interdisciplinary field, the opportunities for further development of coupled design methods and composite manufacturing methods for high performance MNRs will come from scientific discoveries, technological breakthroughs and industrial applications in other fields. Figure 11 depicts the anticipated future trends of high performance MNRs in response to forthcoming application demands, encompassing the realms of design, manufacturing, and testing. In the design phase, a material-structure-function integrated design system based on artificial intelligence (AI) is proposed. In the manufacturing phase, the development of a multi-scale/multi-material AFS-CM process and equipment is suggested. In the testing phase, the function and performance of MNRs are tested and evaluated. Naturally, these three phases operate in parallel, are interconnected, and involve real-time data transfer.

4.2.1. Material-structure-function integrated design system based on AI. In order to break through the shortcomings and limitations of subjective design and the information processing capability of researchers, the future trend lies in the material-structure-function integrated design system based on AI. The system includes the following three aspects: function/performance-oriented AI design software, design parameter and performance digitization method, and functional requirement level evaluation criteria.

The inputs to the function/performance-oriented AI design software are the characteristics and functional requirements of the application environment of the MNRs. The software can explore multiple design possibilities involving multi-factor coupling of material layout, structural innovation, functional integration, and manufacturing process through intelligent algorithms. Moreover, the performance results are predicted and further optimized by integrating multi-physics simulations and other numerical simulations. Finally, the optimal design results for high performance MNRs are output. Therefore, it is necessary to build AI design software to enhance the design capability. However, faced with the diverse results of existing MNRs, there is still lack of scientific methods to standardize and unify the digitization of each design parameter and performance of existing MNRs using standardized formats for data and metadata, leading to the impossibility of accurately constructing a comprehensive database for the training of intelligent algorithms. Therefore, it is necessary to explore methods for digitizing the design parameters and performance of MNRs for AI design software. In addition, given the multifunctional requirements of MNRs to perform tasks, a reasonable judgment of the requirement level for each function is an important reference criterion when the software optimizes the design of MNRs. Therefore, it is necessary to establish scientific and standardized criteria for evaluation of the level of functional requirements for different application areas.

4.2.2. Development of multi-scale/multi-material AFS-CM processes and equipment. In the manufacturing phase, digital design and optimization bring higher requirements to the processes and equipment used to manufacture MNRs. Therefore, the multi-scale/multi-material AFS-CM processes and equipment represent an important trend in the manufacturing phase. The processes and equipment include the following three aspects: multi-scale and multi-material composite manufacturing processes, multifunctional materials for composite

manufacturing, and multi-scale and multi-material composite manufacturing equipment.

The multi-scale composite manufacturing process includes micro-scale and nanoscale, which can fulfill the requirements for the manufacturing of MNRs with micro/nano cross-scale structures. The multi-material composite manufacturing process can fulfill the multi-material/multi-functional manufacturing requirements of MNRs. With DLW based on the two-photon principle as the core, the composite process combining formative and subtractive manufacturing can realize the manufacturing of multi-material, complex micro/nano cross-scale 3D structures. However, the low manufacturing efficiency associated with single-point scanning is a challenge that DLW has to face. Fortunately, the breakthrough in two-color two-step technology has opened up opportunities for the mass manufacturing of MNRs with complex 3D structures [286]. However, it is still constrained by the limited types of multifunctional materials. Multifunctional material selection and design can reduce the complexity of the composite manufacturing process. However, when multifunctional materials are used for manufacturing, the composite process manufacturability of the materials and the manufacturing accuracy should be fully considered. Therefore, the development of multifunctional materials for composite manufacturing is an important area for future research. Based on the above processes and materials, multi-scale and multi-material composite manufacturing equipment is an important hardware foundation for the manufacturing of high performance MNRs. Currently, most of the equipment used for composite manufacturing processes is independent by process step, and this step-by-step approach to manufacturing increases the risk of failure. Therefore, multi-scale and multi-material composite manufacturing equipment is also an important trend in the manufacturing of high performance MNRs.

4.2.3. Testing and evaluation of functionality and performance. To ensure the accuracy and reliability of multi-functional and high performance MNRs, testing and evaluation of functionality and performance are essential. This process encompasses three main aspects: *in-situ* inspection of structure and accuracy, functionality and performance testing equipment, and evaluation and optimization of MNRs.

The development of AI design system and composite manufacturing equipment require higher precision inspection and more complete testing. Since the composite manufacturing process is a combination of multiple manufacturing principles, it is prone to problems such as multi-material bonding defects, unnatural deformation of the structure, and excessive material removal. Therefore, *in-situ* inspection of the structure and accuracy is crucial to ensure the accuracy of the MNRs. In addition, testing functionality and performance is important to validate the capability of MNRs to perform tasks. Targeted test equipment can be designed for different application environments and functionally integrated MNRs, and the results can be fed back to the AI design system and

composite manufacturing equipment in order to further optimize and refine the design software and manufacturing equipment, which ultimately leads to the further optimization of high performance MNRs.

The integration of the above three aspects of design, manufacturing and testing provides more opportunities for the development of high performance MNRs. For example, we envision an integrated system that includes the AI design system, the composite manufacturing equipment, and the *in-situ* inspection system (figure 12). Taking the sensing and high load functions as example, the materials, structures, processes, etc that can realize these functions are designed through AI. For manufacturing, the overall structure is manufactured by a two-color two-step light-curing process, followed by the functional materials coating by a PVD process, the functional material area segmentation by a dry etching process, and finally an array of high specific surface area sensing microstructures is obtained by a droplet-triggered self-rolled process. Meanwhile, in the manufacturing process, the *in-situ* inspection system consists of advanced sensor detection technology [287, 288], high-resolution micro-imaging technology [289], precision micro-operation platforms [290], multi-directional imaging technology [291], and deep learning self-correction system [292, 293]. This system can perform real-time inspection and correction of the MNRs' overall structural shape, surface roughness, internal defects, segmentation area precision, and micro-structural shape. For uncorrectable errors and defects, real-time feedback is provided to the AI design system to make feasible adjustments to the design program. Thus, the entire process (from design and manufacturing to inspection) of information integration is realized.

5. Conclusion

This paper reviews the coupled design methods for high performance MNRs from three aspects, including material-function design, interface-performance design, and structure-performance design. In addition, existing manufacturing methods for MNRs are summarized. The AFS-CM methods for functional structures in MNRs are discussed in detail from the material, structure, function, performance, and process perspectives. These functional structures include Janus spheres, rods, tubes, helices, and some unique structures. Although a wide variety of MNRs have been designed and manufactured, many significant challenges remain. This paper concludes with an exploration of current limitations and prospective future trends. Notably, this paper discusses trends in enhancing high performance MNRs to meet future application requirements through advancements in design, manufacturing, and testing methodologies. An integrated system is proposed as a prospect consisting AI design systems, composite manufacturing equipment, and *in-situ* testing systems. Thus, the summary, discussion, and future trends of this review will greatly contribute to the further development of high performance MNRs and provide valuable guidance for researchers interested in this area.

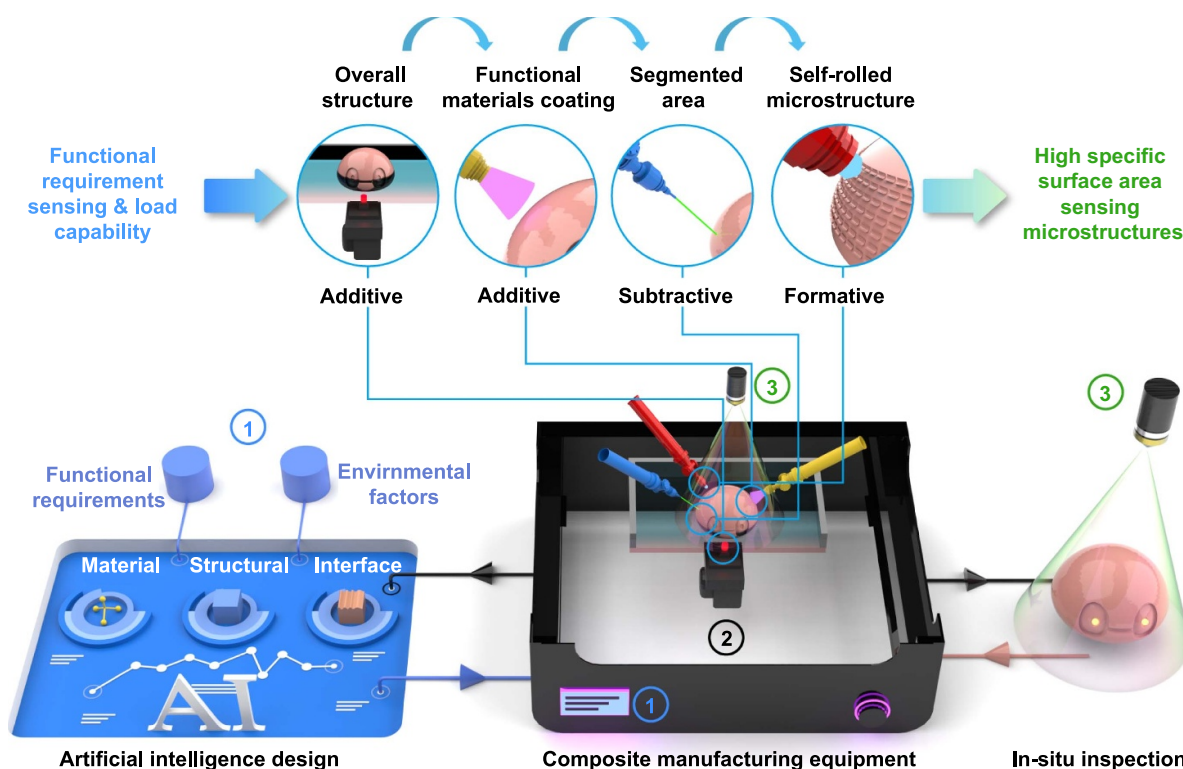


Figure 12. Schematic illustrating the integrated system of AI design system, composite manufacturing equipment and *in-situ* inspection system.

Acknowledgments

This work was supported by the National Natural Science Foundation of China (Nos. 52125505, U23A20637).

ORCID iD

Longqiu Li  <https://orcid.org/0000-0001-9392-527X>

References

- [1] Aziz A, Medina-Sánchez M, Koukourakis N, Wang J, Kuschmierz R, Radner H, Czarske J W and Schmidt O G 2019 Real-time IR tracking of single reflective micromotors through scattering tissues *Adv. Funct. Mater.* **29** 1905272
- [2] Xie L *et al* 2022 Kinetics-controlled super-assembly of asymmetric porous and hollow carbon nanoparticles as light-sensitive smart nanovehicles *J. Am. Chem. Soc.* **144** 1634–46
- [3] Gao Y X, Ou L Y, Liu K F, Guo Y, Li W Y, Xiong Z, Wu C J, Wang J Z, Tang J Y and Li D 2024 Template-guided silicon micromotor assembly for enhanced cell manipulation *Angew. Chem., Int. Ed.* **63** e202405895
- [4] Zhao Y, Yuan M G, Yang H W, Li J, Ying Y L, Li J H, Wang W H and Wang S 2024 Versatile multi-wavelength light-responsive metal-organic frameworks micromotor through porphyrin metalation for water sterilization *Small* **20** 2305189
- [5] Wang W, Castro L A, Hoyos M and Mallouk T E 2012 Autonomous motion of metallic microrods propelled by ultrasound *ACS Nano* **6** 6122–32
- [6] Ahmed D, Baasch T, Jang B, Pane S, Dual J and Nelson B J 2016 Artificial swimmers propelled by acoustically activated flagella *Nano Lett.* **16** 4968–74
- [7] Cao W X, Wei W, Qiu B, Liu Y, Xie S, Fang Q B and Li X H 2024 Ultrasound-powered hydrogen peroxide-responsive Janus micromotors for targeted thrombolysis and recurrence inhibition *Chem. Eng. J.* **483** 149187
- [8] Chen T, Yang J, Zhao H, Li D J, Luo X Y, Fan Z Y, Ren B Y, Cai Y P and Dong R F 2024 Ultrasound-propelled nanomotors for efficient cancer cell ferroptosis *J. Mater. Chem. B* **12** 667–77
- [9] Kim K, Liang Z X, Liu M L and Fan D E 2017 Biobased high-performance rotary micromotors for individually reconfigurable micromachine arrays and microfluidic applications *ACS Appl. Mater. Interfaces* **9** 6144–52
- [10] Yoshizumi Y, Honegger T, Berton K, Suzuki H and Peyrade D 2015 Trajectory control of self-propelled micromotors using AC electrokinetics *Small* **11** 5630–5
- [11] Panda S K, Debata S and Singh D P 2024 Characterizing the Janus colloidal particles in AC electric field and a step towards label-free cargo manipulation *Chem. Phys. Impact* **8** 100588
- [12] Zhang Y B *et al* 2019 Real-time tracking of fluorescent magnetic spore-based microrobots for remote detection of C. diff toxins *Sci. Adv.* **5** eaau9650
- [13] Dong M *et al* 2020 3D-printed soft magnetoelectric microswimmers for delivery and differentiation of neuron-like cells *Adv. Funct. Mater.* **30** 1910323
- [14] Liu S Y, Chen B, Feng Y, Gao C, Du D L, Jiang T T, Tu Y F and Peng F 2024 Helical hydrogel micromotors for

- delivery of neural stem cells and restoration of neural connectivity *Chem. Eng. J.* **479** 147745
- [15] Docampo M A R, Hovorka O and Städler B 2024 Magnetic micromotors crossing lipid membranes *Nanoscale* **16** 2432–43
- [16] Cao Y, Yi H Y, Ge K Y, Gao Y F, Zhang Z C and Feng H H 2024 Additively manufactured customized microhelix motors' bursting motion in mesoscopic tubes for vessel declogging *RSC Adv.* **14** 2720–6
- [17] Chen Q, Xue Y X, Huang Y L, Guo W Y, Wan M M and Shen J 2024 Mg-based micromotors for electrochemical detection of parkinson's disease blood biomarkers *Sens. Actuators B* **402** 135035
- [18] Tolstoy V, Nikitin K, Kuzin A, Zhu F Y, Li X, Goltzman G, Gorin D, Huang G S, Solovov A A and Mei Y F 2024 Rapid synthesis of Pt(0) motors-microscrolls on a nickel surface via H₂PtCl₆-induced galvanic replacement reaction *Chem. Commun.* **60** 3182–5
- [19] Yu X P, Li Y N, Wu J and Ju H X 2014 Motor-based autonomous microsensor for motion and counting immunoassay of cancer biomarker *Anal. Chem.* **86** 4501–7
- [20] Jin Z *et al* 2019 Multifunctional nanorobot system for active therapeutic delivery and synergistic chemo-photothermal therapy *Nano Lett.* **19** 8550–64
- [21] Glahn-Martínez B, Jurado-Sánchez B, Benito-Peña E, Escarpa A and Moreno-Bondi M C 2024 Magnetic Janus micromotors for fluorescence biosensing of tacrolimus in oral fluids *Biosens. Bioelectron.* **244** 115796
- [22] Zhou X, Li Z T, Tan L H, Zhang Y and Jiao Y P 2020 Near-infrared light-steered graphene aerogel micromotor with high speed and precise navigation for active transport and microassembly *ACS Appl. Mater. Interfaces* **12** 23134–44
- [23] Liu X J, Chen W J, Zhao D F, Liu X X, Wang Y, Chen Y D and Ma X 2022 Enzyme-powered hollow nanorobots for active microsampling enabled by thermoresponsive polymer gating *ACS Nano* **16** 10354–63
- [24] Kichatov B, Korshunov A, Sudakov V, Golubkov A and Ryapolov P 2024 Droplet manipulation in liquid flow using of magnetic micromotors for drug delivery and microfluidic systems *Colloids Surf. A* **691** 133891
- [25] Villa K, Krejčová L, Novotný F, Heger Z, Sofer Z and Pumera M 2018 Cooperative multifunctional self-propelled paramagnetic microrobots with chemical handles for cell manipulation and drug delivery *Adv. Funct. Mater.* **28** 1804343
- [26] He Y Z, Wang L F, Zhao M, Fan Z H, Rong W B and Sun L N 2022 Flexible magnetic micropartners for micromanipulation at interfaces *ACS Appl. Mater. Interfaces* **14** 22570–81
- [27] Wan M *et al* 2020 Platelet-derived porous nanomotor for thrombus therapy *Sci. Adv.* **6** eaaz9014
- [28] Stanton M M, Park B W, Vilela D, Bente K, Faivre D, Sitti M and Sánchez S 2017 Magnetotactic bacteria powered biohybrids target *E. coli* biofilms *ACS Nano* **11** 9968–78
- [29] Yan X *et al* 2017 Multifunctional biohybrid magnetite microrobots for imaging-guided therapy *Sci. Robot.* **2** eaaq1155
- [30] Gordón Pidal J M, Arruza L, Moreno-Guzmán M, López M Á and Escarpa A 2024 Micromotor-based dual aptassay for early cost-effective diagnosis of neonatal sepsis *Microchim. Acta* **191** 106
- [31] Yang J H, Zheng J P, Ai R Q, Lai Y H, Chow T H, Shao L and Wang J F 2021 Plasmon-enhanced, self-traced nanomotors on the surface of silicon *Angew. Chem.* **133** 25162–71
- [32] Li J X, Gao W, Dong R F, Pei A, Sattayasamitsathit S and Wang J 2014 Nanomotor lithography *Nat. Commun.* **5** 5026
- [33] Oral C M, Ussia M and Pumera M 2021 Self-propelled activated carbon micromotors for “on-the-fly” capture of nitroaromatic explosives *J. Phys. Chem. C* **125** 18040–5
- [34] Su Y Y, Zhang M J, Wang W, Deng C F, Peng J, Liu Z, Faraj Y, Ju X J, Xie R and Chu L Y 2019 Bubble-propelled hierarchical porous micromotors from evolved double emulsions *Ind. Eng. Chem. Res.* **58** 1590–600
- [35] Dai J, Cheng X, Li X F, Wang Z S, Wang Y F, Zheng J, Liu J, Chen J W, Wu C J and Tang J Y 2021 Solution-synthesized multifunctional Janus nanotree microswimmer *Adv. Funct. Mater.* **31** 2106204
- [36] Chen L, Gan Q B, Xiao X Q, Cai S G, Yan X H and Zheng C 2024 Bio-templated synthesis of MnO₂-based micromotors for enhanced heavy metal removal from aqueous solutions *J. Mater. Sci.* **59** 4267–80
- [37] Muñoz J, Urso M and Pumera M 2022 Self-propelled multifunctional microrobots harboring chiral supramolecular selectors for “enantio-recognition-on-the-fly” *Angew. Chem., Int. Ed.* **61** e202116090
- [38] Gao W, Pei A, Dong R F and Wang J 2014 Catalytic iridium-based Janus micromotors powered by ultralow levels of chemical fuels *J. Am. Chem. Soc.* **136** 2276–9
- [39] Wang J M, Toebes B J, Plachokova A S, Liu Q, Deng D M, Jansen J A, Yang F and Wilson D A 2020 Self-propelled PLGA micromotor with chemotactic response to inflammation *Adv. Healthcare Mater.* **9** 1901710
- [40] Vilela D, Cossío U, Parmar J, Martínez-Villacorta A M, Gómez-Vallejo V, Llop J and Sánchez S 2018 Medical imaging for the tracking of micromotors *ACS Nano* **12** 1220–7
- [41] Patiño T, Feiner-Gracia N, Arqué X, Miguel-López A, Jannasch A, Stumpp T, Schaffer E, Albertazzi L and Sánchez S 2018 Influence of enzyme quantity and distribution on the self-propulsion of non-Janus urease-powered micromotors *J. Am. Chem. Soc.* **140** 7896–903
- [42] Cui D H, Yan Z Y, Chen X W, Liu J Y and Wang W 2024 Electroosmotic flow spin tracers near chemical nano/micromotors *Nanoscale* **16** 2847–51
- [43] Kamankesh M, Kargari Aghmiouni D and Khoee S 2024 Copolymer-coated Au–Pt nanomotors for delivery of disulfiram prodrug *ACS Appl. Nano Mater.* **7** 10056–67
- [44] Zhao Z H, Chen J, Zhan G C, Gu S H, Cong J W, Liu M and Liu Y M 2024 Controlling the collective behaviors of ultrasound-driven nanomotors via frequency regulation *Micromachines* **15** 262
- [45] Gao C Y, Lin Z H, Wang D L, Wu Z G, Xie H and He Q 2019 Red blood cell-mimicking micromotor for active photodynamic cancer therapy *ACS Appl. Mater. Interfaces* **11** 23392–400
- [46] Xu L, Tang Y K, Ye W, Wang Z, Guan Z C, Wen M W and Yu T T 2024 Light-driven micro/nanorobot for biomimetic optical communication *IEEE Robot. Autom. Lett.* **9** 2287–94
- [47] Xiong J Y, Li X, He Z Y, Shi Y, Pan T, Zhu G S, Lu D Y and Xin H B 2024 Light-controlled soft bio-microrobot *Light Sci. Appl.* **13** 55
- [48] Boymelgreen A M, Balli T, Miloh T and Yossifon G 2018 Active colloids as mobile microelectrodes for unified label-free selective cargo transport *Nat. Commun.* **9** 760
- [49] Zhuang R C, Zhou D K, Chang X C, Mo Y, Zhang G Y and Li L Q 2022 Alternating current electric field driven topologically defective micro/nanomotors *Appl. Mater. Today* **26** 101314
- [50] Cao Q Y, Zhang Y F, Tang Y P, Wu C J, Wang J Z and Li D 2024 MOF-based magnetic microrobot swarms for pH-responsive targeted drug delivery *Sci. China Chem.* **67** 1216–23

- [51] Zhou D K, Yue H E, Chang X C, Mo Y, Liu Y, Chang H J and Li L Q 2024 Mimicking motor proteins: wall-guided self-navigation of microwheels *ACS Nano* **18** 8853–62
- [52] Wu J F, Jiao N D, Lin D J, Li N, Ma T Y, Tung S, Cheng W, Wu A H and Liu L Q 2024 Dual-responsive nanorobot-based marsupial robotic system for intracranial cross-scale targeting drug delivery *Adv. Mater.* **36** 2306876
- [53] Zhou Y X, Cao Z Q, Jiang L X, Chen Y, Cui X Y, Wu J R, Xie X, Wang L C and Ying T 2024 Magnetically actuated sonodynamic nanorobot collectives for potentiated ovarian cancer therapy *Front. Bioeng. Biotechnol.* **12** 1374423
- [54] Yu S M *et al* 2024 Magnetic-acoustic actuated spinous microrobot for enhanced degradation of organic pollutants *Ultrason. Sonochem.* **102** 106714
- [55] Ma X, Jang S, Popescu M N, Uspal W E, Miguel-López A, Hahn K, Kim D P and Sánchez S 2016 Reversed Janus micro/nanomotors with internal chemical engine *ACS Nano* **10** 8751–9
- [56] Yasa I C, Ceylan H, Bozuyuk U, Wild A M and Sitti M 2020 Elucidating the interaction dynamics between microswimmer body and immune system for medical microrobots *Sci. Robot.* **5** eaaz3867
- [57] Liao P, Xing L X, Zhang S W and Sun D 2019 Magnetically driven undulatory microswimmers integrating multiple rigid segments *Small* **15** 1901197
- [58] Park J, Kim J Y, Pané S, Nelson B J and Choi H 2021 Acoustically mediated controlled drug release and targeted therapy with degradable 3D porous magnetic microrobots *Adv. Healthcare Mater.* **10** 2001096
- [59] Tang M J, Wang W, Li Z L, Liu Z M, Guo Z Y, Tian H Y, Liu Z, Ju X J, Xie R and Chu L Y 2018 Controllable microfluidic fabrication of magnetic hybrid microswimmers with hollow helical structures *Ind. Eng. Chem. Res.* **57** 9430–8
- [60] Yu Y R, Guo J H, Wang Y T, Shao C M, Wang Y and Zhao Y J 2020 Bioinspired helical micromotors as dynamic cell microcarriers *ACS Appl. Mater. Interfaces* **12** 16097–103
- [61] Cui D H, Lyu X, Duan S F, Peng Y X and Wang W 2022 Rhodium oxide nanorod motors powered by light across the full visible spectrum *ACS Appl. Nano Mater.* **5** 14235–40
- [62] Singh V V, Martin A, Kaufmann K, De Oliveira S D S and Wang J 2015 Zirconia/graphene oxide hybrid micromotors for selective capture of nerve agents *Chem. Mater.* **27** 8162–9
- [63] Li J X, Li T L, Xu T L, Kiristi M, Liu W J, Wu Z G and Wang J 2015 Magneto–acoustic hybrid nanomotor *Nano Lett.* **15** 4814–21
- [64] Soto F, Wagner G L, Garcia-Gradilla V, Gillespie K T, Lakshminpathy D R, Karshalev E, Angell C, Chen Y and Wang J 2016 Acoustically propelled nanoshells *Nanoscale* **8** 17788–93
- [65] Ren J Y, Hu P C, Ma E H, Zhou X Y, Wang W J, Zheng S H and Wang H 2022 Enzyme-powered nanomotors with enhanced cell uptake and lysosomal escape for combined therapy of cancer *Appl. Mater. Today* **27** 101445
- [66] Wang W, Wu Z G, Yang L, Si T Y and He Q 2022 Rational design of polymer conical nanoswimmers with upstream motility *ACS Nano* **16** 9317–28
- [67] Vyskočil J, Mayorga-Martinez C C, Jablonská E, Novotný F, Ruml T and Pumera M 2020 Cancer cells microsurgery via asymmetric bent surface Au/Ag/Ni microrobotic scalpels through a transversal rotating magnetic field *ACS Nano* **14** 8247–56
- [68] X L J *et al* 2016 Enteric micromotor can selectively position and spontaneously propel in the gastrointestinal tract *ACS Nano* **10** 9536–42
- [69] Ye Z H, Wang Y, Liu S H, Xu D D, Wang W and Ma X 2021 Construction of nanomotors with replaceable engines by supramolecular machine-based host–guest assembly and disassembly *J. Am. Chem. Soc.* **143** 15063–72
- [70] Moo J G S, Presolski S and Pumera M 2016 Photochromic spatiotemporal control of bubble-propelled micromotors by a spiropyran molecular switch *ACS Nano* **10** 3543–52
- [71] Ceylan H, Yasa I C, Yasa O, Tabak A F, Giltinan J and Sitti M 2019 3D-printed biodegradable microswimmer for theranostic cargo delivery and release *ACS Nano* **13** 3353–62
- [72] Garcia-Gradilla V, Orozco J, Sattayasamitsathit S, Soto F, Kuralay F, Pourazary A, Katzenberg A, Gao W, Shen Y F and Wang J 2013 Functionalized ultrasound-propelled magnetically guided nanomotors: toward practical biomedical applications *ACS Nano* **7** 9232–40
- [73] Wu Z G, Li T L, Gao W, Xu T L, Jurado-sánchez B, Li J X, Gao W W, He Q, Zhang L F and Wang J 2015 Cell-membrane-coated synthetic nanomotors for effective biotransformation *Adv. Funct. Mater.* **25** 3881–7
- [74] Jang B *et al* 2015 Undulatory locomotion of magnetic multilink nanoswimmers *Nano Lett.* **15** 4829–33
- [75] Ji F T, Li T L, Yu S M, Wu Z G and Zhang L 2021 Propulsion gait analysis and fluidic trapping of swinging flexible nanomotors *ACS Nano* **15** 5118–28
- [76] Zheng Z Q, Wang H P, Dong L X, Shi Q, Li J N, Sun T, Huang Q and Fukuda T 2021 Ionic shape-morphing microrobotic end-effectors for environmentally adaptive targeting, releasing, and sampling *Nat. Commun.* **12** 411
- [77] Lin X Y *et al* 2021 Flying squirrel-inspired motion control of a light-deformed Pt-PazoMA micromotor through drag force manipulation *ACS Appl. Mater. Interfaces* **13** 30106–17
- [78] Maria-Hormigos R, Jurado-Sanchez B, Vazquez L and Escarpa A 2016 Carbon allotrope nanomaterials based catalytic micromotors *Chem. Mater.* **28** 8962–70
- [79] Yuan K S, De La Asunción-Nadal V, Li Y L, Jurado-Sánchez B and Escarpa A 2020 Graphdiyne tubular micromotors: electrosynthesis, characterization and self-propelled capabilities *Appl. Mater. Today* **20** 100743
- [80] Maric T, Nasir M Z M, Webster R D and Pumera M 2020 Tailoring metal/TiO₂ interface to influence motion of light-activated Janus micromotors *Adv. Funct. Mater.* **30** 1908614
- [81] Valdez-Garduño M, Leal-Estrada M, Oliveros-Mata E S, Sandoval-Bojorquez D I, Soto F, Wang J and Garcia-Gradilla V 2020 Density asymmetry driven propulsion of ultrasound-powered Janus micromotors *Adv. Funct. Mater.* **30** 2004043
- [82] Zhou M F, Hou T, Li J X, Yu S S, Xu Z J, Yin M, Wang J and Wang X L 2019 Self-propelled and targeted drug delivery of poly(aspartic acid)/iron–zinc microrocket in the stomach *ACS Nano* **13** 1324–32
- [83] Maric T, Nasir M Z M, Rosli N F, Budanović M, Webster R D, Cho N J and Pumera M 2020 Microrobots derived from variety plant pollen grains for efficient environmental clean up and as an anti-cancer drug carrier *Adv. Funct. Mater.* **30** 2000112
- [84] Hortelão A C, Carrascosa R, Murillo-Cremaes N, Patiño T and Sánchez S 2019 Targeting 3D bladder cancer spheroids with urease-powered nanomotors *ACS Nano* **13** 429–39
- [85] Wang L, Hortelão A C, Huang X and Sánchez S 2019 Lipase-powered mesoporous silica nanomotors for triglyceride degradation *Angew. Chem., Int. Ed.* **58** 7992–6
- [86] Wang J, Si J W, Li J Y, Zhang P P, Wang Y, Zhang W, Jin B, Li W Q, Li N and Miao S D 2021 Self-propelled nanojets for fenton catalysts based on halloysite with embedded Pt

- and outside-grafted Fe₃O₄ *ACS Appl. Mater. Interfaces* **13** 49017–26
- [87] Liu W J, Chen X, Lu X L, Wang J, Zhang Y N and Gu Z W 2020 From passive inorganic oxides to active matters of micro/nanomotors *Adv. Funct. Mater.* **30** 2003195
- [88] Wang S N, Liu X J, Wang Y, Xu D D, Liang C Y, Guo J H and Ma X 2019 Biocompatibility of artificial micro/nanomotors for use in biomedicine *Nanoscale* **11** 14099–112
- [89] Hermanová S and Pumera M 2018 Polymer platforms for micro- and nanomotor fabrication *Nanoscale* **10** 7332–42
- [90] Soto F, Karshalev E, Zhang F Y, Esteban Fernandez De Avila B, Nourhani A and Wang J 2022 Smart materials for microrobots *Chem. Rev.* **122** 5365–403
- [91] Chen C R, Ding S C and Wang J 2024 Materials consideration for the design, fabrication and operation of microscale robots *Nat. Rev. Mater.* **9** 159–72
- [92] Chen X Z, Hoop M, Mushtaq F, Siringil E, Hu C Z, Nelson B J and Pané S 2017 Recent developments in magnetically driven micro- and nanorobots *Appl. Mater. Today* **9** 37–48
- [93] Katuri J, Ma X, Stanton M M and Sánchez S 2017 Designing micro- and nanoswimmers for specific applications *Acc. Chem. Res.* **50** 2–11
- [94] Sánchez S, Soler L and Katuri J 2015 Chemically powered micro- and nanomotors *Angew. Chem., Int. Ed.* **54** 1414–44
- [95] Ren Z and Gao P X 2014 A review of helical nanostructures: growth theories, synthesis strategies and properties *Nanoscale* **6** 9366–400
- [96] Banno T, Ueno K, Kojima T and Asakura K 2024 Induction for self-propelled motion of artificial objects with/without shape anisotropy *J. Oleo Sci.* **73** 509–18
- [97] Xu B R, Zhang B R, Wang L, Huang G S and Mei Y F 2018 Tubular micro/nanomachines: from the basics to recent advances *Adv. Funct. Mater.* **28** 1705872
- [98] Zhang X, Fu Q R, Duan H W, Song J B and Yang H H 2021 Janus nanoparticles: from fabrication to (bio)applications *ACS Nano* **15** 6147–91
- [99] Fu J Y, An D, Song Y L, Wang C, Qiu M and Zhang H 2020 Janus nanoparticles for cellular delivery chemotherapy: recent advances and challenges *Coord. Chem. Rev.* **422** 213467
- [100] Wang H and Pumera M 2015 Fabrication of micro/nanoscale motors *Chem. Rev.* **115** 8704–35
- [101] Ye J M, Fan Y Y, Niu G L, Zhou B L, Kang Y and Ji X Y 2024 Intelligent micro/nanomotors: fabrication, propulsion, and biomedical applications *Nano Today* **55** 102212
- [102] Liu D, Wang T and Lu Y 2022 Untethered microrobots for active drug delivery: from rational design to clinical settings *Adv. Healthcare Mater.* **11** 2102253
- [103] Xu D D, Wang Y, Liang C Y, You Y Q, Sanchez S and Ma X 2020 Self-propelled micro/nanomotors for on-demand biomedical cargo transportation *Small* **16** 1902464
- [104] Gao C, Feng Y, Wilson D A, Tu Y F and Peng F 2022 Micro-Nano motors with taxis behavior: principles, designs, and biomedical applications *Small* **18** 2106263
- [105] Zhou C C, Deng J Y, Hao Tay J, Basu S, Yang J Y, Li J, Yang C M, Zhao Z and Cho N J 2024 Multifunctional material building blocks from plant pollen *Annu. Rev. Chem. Biomol.* **15** 1–24
- [106] Chen T, Cai Y P, Ren B Y, Sánchez B J and Dong R F 2024 Intelligent micro/nanorobots based on biotemplates *Mater. Horiz.* **11** 2772–801
- [107] Koleoso M, Feng X, Xue Y, Li Q, Munshi T and Chen X 2020 Micro/nanoscale magnetic robots for biomedical applications *Mater. Today Bio* **8** 100085
- [108] Ou J F, Liu K, Jiang J M, Wilson D A, Liu L, Wang F, Wang S H, Tu Y F and Peng F 2020 Micro-/nanomotors toward biomedical applications: the recent progress in biocompatibility *Small* **16** 1906184
- [109] Ye H, Wang Y, Xu D D, Liu X J, Liu S M and Ma X 2021 Design and fabrication of micro/Nano-motors for environmental and sensing applications *Appl. Mater. Today* **23** 101007
- [110] Peng F, Tu Y F and Wilson D A 2017 Micro/nanomotors towards *in vivo* application: cell, tissue and biofluid *Chem. Soc. Rev.* **46** 5289–310
- [111] Dutta S, Noh S, Gual R S, Chen X Z, Pané S, Nelson B J and Choi H 2024 Recent developments in metallic degradable micromotors for biomedical and environmental remediation applications *Nano-Micro. Lett.* **16** 41
- [112] Wang Q Q, Zhang J C, Yu J F, Lang J, Lyu Z, Chen Y F and Zhang L 2023 Untethered small-scale machines for microrobotic manipulation: from individual and multiple to collective machines *ACS Nano* **17** 13081–109
- [113] Wang Q Q, Yang S H and Zhang L 2024 Untethered micro/nanorobots for remote sensing: toward intelligent platform *Nano-Micro. Lett.* **16** 40
- [114] Gao W, Dong R F, Thamphiwatana S, Li J X, Gao W W, Zhang L F and Wang J 2015 Artificial micromotors in the mouse's stomach: a step toward *in vivo* use of synthetic motors *ACS Nano* **9** 117–23
- [115] Wei X L, Beltrán-Gastélum M, Karshalev E, Esteban-fernández De Ávila B, Zhou J R, Ran D N, Angsantikul P, Fang R H, Wang J and Zhang L F 2019 Biomimetic micromotor enables active delivery of antigens for oral vaccination *Nano Lett.* **19** 1914–21
- [116] Gao W, D'Agostino M, Garcia-Gradilla V, Orozco J and Wang J 2013 Multi-fuel driven Janus micromotors *Small* **9** 467–71
- [117] Lu X L, Shen H, Wei Y, Ge H B, Wang J, Peng H M and Liu W J 2020 Ultrafast growth and locomotion of dandelion-like microswarms with tubular micromotors *Small* **16** 2003678
- [118] Gao C Y, Zhou C, Lin Z H, Yang M C and He Q 2019 Surface wettability-directed propulsion of glucose-powered nanoflask motors *ACS Nano* **13** 12758–66
- [119] Hortelão A C, Patiño T, Perez-Jiménez A, Blanco À and Sánchez S 2018 Enzyme-powered nanobots enhance anticancer drug delivery *Adv. Funct. Mater.* **28** 1705086
- [120] Park B W, Zhuang J, Yasa O and Sitti M 2017 Multifunctional bacteria-driven microswimmers for targeted active drug delivery *ACS Nano* **11** 8910–23
- [121] Xin H B, Zhao N, Wang Y N, Zhao X T, Pan T, Shi Y and Li B J 2020 Optically controlled living micromotors for the manipulation and disruption of biological targets *Nano Lett.* **20** 7177–85
- [122] Du S N, Wang H G, Zhou C, Wang W and Zhang Z X 2020 Motor and rotor in one: light-active ZnO/Au twinned rods of tunable motion modes *J. Am. Chem. Soc.* **142** 2213–7
- [123] Lee J G, Al Harraq A, Bishop K J M and Bharti B 2021 Fabrication and electric field-driven active propulsion of patchy microellipsoids *J. Phys. Chem. B* **125** 4232–40
- [124] Wu Y, Fu A F and Yossifon G 2020 Active particles as mobile microelectrodes for selective bacteria electroporation and transport *Sci. Adv.* **6** eaay4412
- [125] Akolpoglu M B, Alapan Y, Dogan N O, Baltaci S F, Yasa O, Aybar Tural G and Sitti M 2022 Magnetically steerable bacterial microrobots moving in 3D biological matrices for stimuli-responsive cargo delivery *Sci. Adv.* **8** eabo6163
- [126] Zheng S H, Wang Y, Pan S H, Ma E H, Jin S, Jiao M, Wang W J, Li J J, Xu K and Wang H 2021 Biocompatible nanomotors as active diagnostic imaging agents for enhanced magnetic resonance imaging of tumor tissues *in vivo Adv. Funct. Mater.* **31** 2100936
- [127] Ren L Q, Zhou D K, Mao Z M, Xu P T, Huang T J and Mallouk T E 2017 Rheotaxis of bimetallic micromotors

- driven by chemical–acoustic hybrid power *ACS Nano* **11** 10591–8
- [128] Li T L, Zhang A N, Shao G B, Wei M S, Guo B, Zhang G Y, Li L Q and Wang W 2018 Janus microdimer surface walkers propelled by oscillating magnetic fields *Adv. Funct. Mater.* **28** 1706066
- [129] Mayorga-Martinez C C, Fojtů M, Vyskočil J, Cho N J and Pumera M 2022 Pollen-based magnetic microrobots are mediated by electrostatic forces to attract, manipulate, and kill cancer cells *Adv. Funct. Mater.* **32** 2207272
- [130] Wang X P, Qin X H, Hu C Z, Terzopoulou A, Chen X Z, Huang T Y, Maniura-Weber K, Pané S and Nelson B J 2018 3D printed enzymatically biodegradable soft helical microswimmers *Adv. Funct. Mater.* **28** 1804107
- [131] Yue H E, Chang X C, Liu J M, Zhou D K and Li L Q 2022 Wheel-like magnetic-driven microswarm with a band-aid imitation for patching up microscale intestinal perforation *ACS Appl. Mater. Interfaces* **14** 8743–52
- [132] Wang Q Q, Du X Z, Jin D D and Zhang L 2022 Real-time ultrasound doppler tracking and autonomous navigation of a miniature helical robot for accelerating thrombolysis in dynamic blood flow *ACS Nano* **16** 604–16
- [133] Wang Q L *et al* 2024 Tracking and navigation of a microswarm under laser speckle contrast imaging for targeted delivery *Sci. Robot.* **9** eadh1978
- [134] Wang Q Q, Chan K F, Schweizer K, Du X Z, Jin D D, Yu S C H, Nelson B J and Zhang L 2021 Ultrasound doppler-guided real-time navigation of a magnetic microswarm for active endovascular delivery *Sci. Adv.* **7** eabe5914
- [135] Alapan Y, Bozuyuk U, Erkoç P, Karacakol A C and Sitti M 2020 Multifunctional surface microrollers for targeted cargo delivery in physiological blood flow *Sci. Robot.* **5** eaba5726
- [136] Liu M, Pan L Q, Piao H, Sun H Y, Huang X F, Peng C D and Liu Y M 2015 Magnetically actuated wormlike nanomotors for controlled cargo release *ACS Appl. Mater. Interfaces* **7** 26017–21
- [137] Ji Y X, Lin X K, Zhang H Y, Wu Y J, Li J B and He Q 2019 Thermoresponsive polymer brush modulation on the direction of motion of phoretically driven Janus micromotors *Angew. Chem.* **131** 4228–32
- [138] Gordón J, Arruza L, Ibáñez M D, Moreno-Guzmán M, López M Á and Escarpa A 2022 On the move-sensitive fluorescent aptassay on board catalytic micromotors for the determination of interleukin-6 in ultra-low serum volumes for neonatal sepsis diagnostics *ACS Sens.* **7** 3144–52
- [139] Esteban-fernández De Ávila B, Lopez-Ramirez M A, Báez D F, Jodra A, Singh V V, Kaufmann K and Wang J 2016 Aptamer-modified graphene-based catalytic micromotors: off-on fluorescent detection of ricin *ACS Sens.* **1** 217–21
- [140] Yuan K S, De La Asuncion-Nadal V, Jurado-Sánchez B and Escarpa A 2020 2D nanomaterials wrapped Janus micromotors with built-in multiengines for bubble, magnetic, and light driven propulsion *Chem. Mater.* **32** 1983–92
- [141] Zhou L, Zhang H W, Bao H M, Wei Y, Fu H and Cai W P 2020 Monodispersed snowman-like Ag-MoS₂ Janus nanoparticles as chemically self-propelled nanomotors *ACS Appl. Nano Mater.* **3** 624–32
- [142] De La Asunción-Nadal V, Pacheco M, Jurado-Sánchez B and Escarpa A 2020 Chalcogenides-based tubular micromotors in fluorescent assays *Anal. Chem.* **92** 9188–93
- [143] Maric T, Nasir M Z M, Mayorga-Martinez C C, Rosli N F, Budanović M, Szökölóvá K I, Webster R D, Sofer Z and Pumera M 2019 Cloisite microrobots as self-propelling cleaners for fast and efficient removal of improvised organophosphate nerve agents *ACS Appl. Mater. Interfaces* **11** 31832–43
- [144] Singh V V, Jurado-Sánchez B, Sattayasamitsathit S, Orozco J, Li J X, Galarnyk M, Fedorak Y and Wang J 2015 Multifunctional silver-exchanged zeolite micromotors for catalytic detoxification of chemical and biological threats *Adv. Funct. Mater.* **25** 2147–55
- [145] Liu X X, Sun X, Peng Y X, Wang Y, Xu D D, Chen W J, Wang W, Yan X H and Ma X 2022 Intrinsic properties enabled metal organic framework micromotors for highly efficient self-propulsion and enhanced antibacterial therapy *ACS Nano* **16** 14666–78
- [146] Ma X, Wang X, Hahn K and Sánchez S 2016 Motion control of urea-powered biocompatible hollow microcapsules *ACS Nano* **10** 3597–605
- [147] Li J Y, Li X J, Luo T, Wang R, Liu C C, Chen S X, Li D F, Yue J B, Cheng S H and Sun D 2018 Development of a magnetic microrobot for carrying and delivering targeted cells *Sci. Robot.* **3** eaat8829
- [148] Wu Z G, Lin X K, Zou X, Sun J M and He Q 2015 Biodegradable protein-based rockets for drug transportation and light-triggered release *ACS Appl. Mater. Interfaces* **7** 250–5
- [149] Bernasconi R, Mauri E, Rossetti A, Rimondo S, Suriano R, Levi M, Sacchetti A, Pané S, Magagnin L and Rossi F 2021 3D integration of pH-cleavable drug-hydrogel conjugates on magnetically driven smart microtransporters *Mater. Des.* **197** 109212
- [150] Lu X L, Ou H, Wei Y, Ding X Y, Wang X, Zhao C, Bao J H and Liu W J 2022 Superfast fuel-free tubular hydrophobic micromotors powered by ultrasound *Sens. Actuators B* **372** 132667
- [151] Chang X C, Li L Q, Li T L, Zhou D K and Zhang G Y 2016 Accelerated microrockets with a biomimetic hydrophobic surface *RSC Adv.* **6** 87213–20
- [152] Zhou M Y, Xing Y, Li X Y, Du X, Xu T L and Zhang X J 2020 Cancer cell membrane camouflaged semi-yolk@spiky-shell nanomotor for enhanced cell adhesion and synergistic therapy *Small* **16** 2003834
- [153] Go G *et al* 2021 Multifunctional biodegradable microrobot with programmable morphology for biomedical applications *ACS Nano* **15** 1059–76
- [154] Yang Q X, Tang S S, Lu D D, Li Y Y, Wan F C, Li J H, Chen Q W, Cong Z Q, Zhang X J and Wu S 2022 Pollen typhae-based magnetic-powered microrobots toward acute gastric bleeding treatment *ACS Appl. Bio Mater.* **5** 4425–34
- [155] Gao L, Zhang K and Chen Y M 2012 Dumpling-like nanocomplexes of foldable Janus polymer sheets and spheres *ACS Macro Lett.* **1** 1143–5
- [156] Goodarzi H, Jadidi K, Pourmotabed S, Sharifi E and Aghamollaei H 2019 Preparation and *in vitro* characterization of cross-linked collagen–gelatin hydrogel using EDC/NHS for corneal tissue engineering applications *Int. J. Biol. Macromol.* **126** 620–32
- [157] Simmchen J, Baeza A, Ruiz-Molina D and Vallet-Regí M 2014 Improving catalase-based propelled motor endurance by enzyme encapsulation *Nanoscale* **6** 8907–13
- [158] Singh A V, Hosseindoust Z, Park B W, Yasa O and Sitti M 2017 Microemulsion-based soft bacteria-driven microswimmers for active cargo delivery *ACS Nano* **11** 9759–69
- [159] Luo M, Li S L, Wan J S, Yang C L, Chen B D and Guan J G 2020 Enhanced propulsion of urease-powered micromotors by multilayered assembly of ureases on Janus magnetic microparticles *Langmuir* **36** 7005–13
- [160] Singh D P, Uspal W E, Popescu M N, Wilson L G and Fischer P 2018 Photogravitactic microswimmers *Adv. Funct. Mater.* **28** 1706660

- [161] Yang Q X, Xu H Y, Wen H T, Zhao H, Liu X Y, Cai Y P, Wang H and Dong R F 2021 Graphene oxide induced enhancement of light-driven micromotor with biocompatible fuels *Appl. Mater. Today* **22** 100943
- [162] Urso M, Ussia M and Pumera M 2023 Smart micro- and nanorobots for water purification *Nat. Rev. Bioeng.* **1** 236–51
- [163] Das S, Garg A, Campbell A I, Howse J, Sen A, Velegol D, Golestanian R and Ebbens S J 2015 Boundaries can steer active Janus spheres *Nat. Commun.* **6** 8999
- [164] Chen X, Xu Y K, Zhou C, Lou K, Peng Y X, Zhang H P and Wang W 2022 Unraveling the physiochemical nature of colloidal motion waves among silver colloids *Sci. Adv.* **8** eabn9130
- [165] Aziz A, Holthof J, Meyer S, Schmidt O G and Medina-Sánchez M 2021 Dual ultrasound and photoacoustic tracking of magnetically driven micromotors: from *in vitro* to *in vivo* *Adv. Healthcare Mater.* **10** 2101077
- [166] Guo J H, Gallegos J J, Tom A R and Fan D L 2018 Electric-field-guided precision manipulation of catalytic nanomotors for cargo delivery and powering nanoelectromechanical devices *ACS Nano* **12** 1179–87
- [167] Liu M H *et al* 2022 Light-driven Au–ZnO nanorod motors for enhanced photocatalytic degradation of tetracycline *Nanoscale* **14** 12804–13
- [168] Kim K, Xu X B, Guo J H and Fan D L 2014 Ultrahigh-speed rotating nanoelectromechanical system devices assembled from nanoscale building blocks *Nat. Commun.* **5** 3632
- [169] L L T *et al* 2016 Magnetically propelled fish-like nanoswimmers *Small* **12** 6098–105
- [170] Xu X B, Kim K and Fan D L 2015 Tunable release of multiplex biochemicals by plasmonically active rotary nanomotors *Angew. Chem.* **127** 2555–9
- [171] Wang H, Moo J G S and Pumera M 2016 From nanomotors to micromotors: the influence of the size of an autonomous bubble-propelled device upon its motion *ACS Nano* **10** 5041–50
- [172] Lee S, Kim S, Kim S, Kim J Y, Moon C, Nelson B J and Choi H 2018 A capsule-type microrobot with pick-and-drop motion for targeted drug and cell delivery *Adv. Healthcare Mater.* **7** 1700985
- [173] Lee S, Kim J Y, Kim J, Hoshiar A K, Park J, Lee S, Kim J, Pané S, Nelson B J and Choi H 2020 A needle-type microrobot for targeted drug delivery by affixing to a microtissue *Adv. Healthcare Mater.* **9** 1901697
- [174] Chen Y D *et al* 2022 Carbon helical nanorobots capable of cell membrane penetration for single cell targeted SERS bio-sensing and photothermal cancer therapy *Adv. Funct. Mater.* **32** 2200600
- [175] Medina-Sánchez M, Schwarz L, Meyer A K, Hebenstreit F and Schmidt O G 2016 Cellular cargo delivery: toward assisted fertilization by sperm-carrying micromotors *Nano Lett.* **16** 555–61
- [176] Pourrahimi A M, Villa K, Manzanares Palenzuela C L, Ying Y L, Sofer Z and Pumera M 2019 Catalytic and light-driven ZnO/Pt Janus Nano/micromotors: switching of motion mechanism via interface roughness and defect tailoring at the nanoscale *Adv. Funct. Mater.* **29** 1808678
- [177] Pourrahimi A M, Villa K, Ying Y L, Sofer Z and Pumera M 2018 ZnO/ZnO₂/Pt Janus micromotors propulsion mode changes with size and interface structure: enhanced nitroaromatic explosives degradation under visible light *ACS Appl. Mater. Interfaces* **10** 42688–97
- [178] Palacci J, Sacanna S, Vatchinsky A, Chaikin P M and Pine D J 2013 Photoactivated colloidal dockers for cargo transportation *J. Am. Chem. Soc.* **135** 15978–81
- [179] Zheng C, Li Z Q, Xu T T, Chen L, Fang F, Wang D, Dai P Q, Wang Q T, Wu X Y and Yan X H 2021 *Spirulina*-templated porous hollow carbon@magnetite core-shell microswimmers *Appl. Mater. Today* **22** 100962
- [180] Kim E, Jeon S, An H K, Kianpour M, Yu S W, Kim J Y, Rah J C and Choi H 2020 A magnetically actuated microrobot for targeted neural cell delivery and selective connection of neural networks *Sci. Adv.* **6** eabb5696
- [181] Wang W, Wu Z G, Lin X K, Si T Y and He Q 2019 Gold-nanoshell-functionalized polymer nanoswimmer for photomechanical poration of single-cell membrane *J. Am. Chem. Soc.* **141** 6601–8
- [182] Esteban-Fernández De Ávila B, Lopez-ramirez M A, Mundaca-uribe R, Wei X L, Ramírez-herrera D E, Karshalev E, Nguyen B, Fang R H, Zhang L F and Wang J 2020 Multicompartment tubular micromotors toward enhanced localized active delivery *Adv. Mater.* **32** 2000091
- [183] Li T L, Li J X, Morozov K I, Wu Z G, Xu T L, Rozen I, Leshansky A M, Li L Q and Wang J 2017 Highly efficient freestyle magnetic nanoswimmer *Nano Lett.* **17** 5092–8
- [184] Fan X J, Sun M M, Sun L N and Xie H 2020 Ferrofluid droplets as liquid microrobots with multiple deformabilities *Adv. Funct. Mater.* **30** 2000138
- [185] Liu M, Wang Y X, Kuai Y B, Cong J W, Xu Y L, Piao H G, Pan L Q and Liu Y M 2019 Magnetically powered shape-transformable liquid metal micromotors *Small* **15** 1905446
- [186] Xin C *et al* 2021 Environmentally adaptive shape-morphing microrobots for localized cancer cell treatment *ACS Nano* **15** 18048–59
- [187] Ghosh A *et al* 2020 Gastrointestinal-resident, shape-changing microdevices extend drug release *in vivo* *Sci. Adv.* **6** eabb4133
- [188] Gao W, Feng X M, Pei A, Gu Y E, Li J X and Wang J 2013 Seawater-driven magnesium based Janus micromotors for environmental remediation *Nanoscale* **5** 4696–700
- [189] Gao W, Pei A and Wang J 2012 Water-driven micromotors *ACS Nano* **6** 8432–8
- [190] Chen Q W, Tang S S, Li Y Y, Cong Z Q, Lu D D, Yang Q X, Zhang X J and Wu S 2021 Multifunctional metal–organic framework exoskeletons protect biohybrid sperm microrobots for active drug delivery from the surrounding threats *ACS Appl. Mater. Interfaces* **13** 58382–92
- [191] Deng Q Q, Zhang L, Lv W, Liu X M, Ren J S and Qu X G 2021 Biological mediator-propelled nanosweeper for nonpharmaceutical thrombus therapy *ACS Nano* **15** 6604–13
- [192] Xiang Z C, Jiang G X, Fan D, Tian J S, Hu Z Y and Fang Q J 2020 Drug-internalized bacterial swimmers for magnetically manipulable tumor-targeted drug delivery *Nanoscale* **12** 13513–22
- [193] Wang Q L, Dong R F, Wang C, Xu S Y, Chen D C, Liang Y Y, Ren B Y, Gao W and Cai Y P 2019 Glucose-fueled micromotors with highly efficient visible-light photocatalytic propulsion *ACS Appl. Mater. Interfaces* **11** 6201–7
- [194] Wang K, Wang W J, Pan S H, Fu Y M, Dong B and Wang H 2020 Fluorescent self-propelled covalent organic framework as a microsensor for nitro explosive detection *Appl. Mater. Today* **19** 100550
- [195] Zheng J R, Qi R Q, Dai C L, Li G and Sang M M 2022 Enzyme catalysis biomotor engineering of neutrophils for nanodrug delivery and cell-based thrombolytic therapy *ACS Nano* **16** 2330–44
- [196] Li X R, Zhang B Y, Jakobi T, Yu Z L, Ren L Q and Zhang Z H 2024 Laser-based bionic manufacturing *Int. J. Extrem Manuf.* **6** 042003

- [197] Lian Z X, Zhou J H, Ren W F, Chen F Z, Xu J K, Tian Y L and Yu H D 2024 Recent progress in bio-inspired macrostructure array materials with special wettability— from surface engineering to functional applications *Int. J. Extrem. Manuf.* **6** 012008
- [198] Huang Z Y, Shao G B and Li L Q 2023 Micro/Nano functional devices fabricated by additive manufacturing *Prog. Mater. Sci.* **131** 101020
- [199] Zolfaghari A, Chen T T and Yi A Y 2019 Additive manufacturing of precision optics at micro and nanoscale *Int. J. Extrem. Manuf.* **1** 012005
- [200] Sui S *et al* 2023 Additive manufacturing of magnesium and its alloys: process-formability-microstructure-performance relationship and underlying mechanism *Int. J. Extrem. Manuf.* **5** 042009
- [201] Huang Z Y, Shao G B, Zhou D K, Deng X H, Qiao J and Li L Q 2023 3D printing of high-precision and ferromagnetic functional devices *Int. J. Extrem. Manuf.* **5** 035501
- [202] Feng Y W, Chang X C, Liu H, Hu Y, Li T L and Li L Q 2021 Multi-response biocompatible Janus micromotor for ultrasonic imaging contrast enhancement *Appl. Mater. Today* **23** 101026
- [203] Llopis-Lorente A, García-Fernández A, Murillo-Cremaes N, Hortelão A C, Patiño T, Villalonga R, Sancenón F, Martínez-Máñez R and Sánchez S 2019 Enzyme-powered gated mesoporous silica nanomotors for on-command intracellular payload delivery *ACS Nano* **13** 12171–83
- [204] Ramos-Docampo M A, Fernández-Medina M, Taipaleenmäki E, Hovorka O, Salgueiriño V and Städler B 2019 Microswimmers with heat delivery capacity for 3D cell spheroid penetration *ACS Nano* **13** 12192–205
- [205] Wu Y J, Wu Z G, Lin X K, He Q and Li J B 2012 Autonomous movement of controllable assembled Janus capsule motors *ACS Nano* **6** 10910–6
- [206] Huang W J, Manjare M and Zhao Y P 2013 Catalytic nanoshell micromotors *J. Phys. Chem. C* **117** 21590–6
- [207] Xuan M J, Shao J X, Gao C Y, Wang W, Dai L R and He Q 2018 Self-propelled nanomotors for thermomechanically percolating cell membranes *Angew. Chem., Int. Ed.* **57** 12463–7
- [208] Karshalev E *et al* 2019 Micromotors for active delivery of minerals toward the treatment of iron deficiency anemia *Nano Lett.* **19** 7816–26
- [209] Karshalev E, Esteban-Fernández De Ávila B, Beltrán-Gastélum M, Angsantikul P, Tang S S, Mundaca-Uribe R, Zhang F Y, Zhao J, Zhang L F and Wang J 2018 Micromotor pills as a dynamic oral delivery platform *ACS Nano* **12** 8397–405
- [210] Jang B *et al* 2016 Catalytic locomotion of core-shell nanowire motors *ACS Nano* **10** 9983–91
- [211] Li J X *et al* 2018 Biomimetic platelet-camouflaged nanorobots for binding and isolation of biological threats *Adv. Mater.* **30** 1704800
- [212] Dong Y, Wang L, Wang J, Wang S J, Wang Y, Jin D D, Chen P, Du W, Zhang L and Liu B F 2020 Graphene-based helical micromotors constructed by “microscale liquid rope-coil effect” with microfluidics *ACS Nano* **14** 16600–13
- [213] Dong Y *et al* 2022 Endoscope-assisted magnetic helical micromachine delivery for biofilm eradication in tympanostomy tube *Sci. Adv.* **8** eabq8573
- [214] Ren L Q, Nama N, McNeill J M, Soto F, Yan Z F, Liu W, Wang W, Wang J and Mallouk T E 2019 3D steerable, acoustically powered microswimmers for single-particle manipulation *Sci. Adv.* **5** eaax3084
- [215] Aghakhani A, Pena-Francesch A, Bozuyuk U, Cetin H, Wrede P and Sitti M 2022 High shear rate propulsion of acoustic microrobots in complex biological fluids *Sci. Adv.* **8** eabm5126
- [216] Cao S P, Wu H L, Pijpers I A B, Shao J X, Abdelmohsen L K E A, Williams D S and Van Hest J C M 2021 Cucurbit-like polymersomes with aggregation-induced emission properties show enzyme-mediated motility *ACS Nano* **15** 18270–8
- [217] Guo Z Y, Wu Y F, Xie Z Z, Shao J M, Liu J, Yao Y, Wang J, Shen Y S, Gooding J J and Liang K 2022 Self-propelled initiative collision at microelectrodes with vertically mobile micromotors *Angew. Chem., Int. Ed.* **61** e202209747
- [218] Esteban-Fernández De Ávila B, Angsantikul P, Ramírez-Herrera D E, Soto F, Teymourian H, Dehaini D, Chen Y J, Zhang L F and Wang J 2018 Hybrid biomembrane-functionalized nanorobots for concurrent removal of pathogenic bacteria and toxins *Sci. Robot.* **3** eaat0485
- [219] Zhang F Y *et al* 2022 Nanoparticle-modified microrobots for *in vivo* antibiotic delivery to treat acute bacterial pneumonia *Nat. Mater.* **21** 1324–32
- [220] Gong D, Celi N, Zhang D Y and Cai J 2022 Magnetic biohybrid microrobot multimers based on *Chlorella* cells for enhanced targeted drug delivery *ACS Appl. Mater. Interfaces* **14** 6320–30
- [221] Alapan Y, Yasa O, Schauer O, Giltinan J, Tabak A F, Sourjik V and Sitti M 2018 Soft erythrocyte-based bacterial microswimmers for cargo delivery *Sci. Robot.* **3** eaar4423
- [222] Yao K, Manjare M, Barrett C A, Yang B, Salguero T T and Zhao Y P 2012 Nanostructured scrolls from graphene oxide for microjet engines *J. Phys. Chem. Lett.* **3** 2204–8
- [223] Li J X, Liu Z Q, Huang G S, An Z H, Chen G, Zhang J, Li M L, Liu R and Mei Y F 2014 Hierarchical nanoporous microtubes for high-speed catalytic microengines *NPG Asia Mater.* **6** e94
- [224] Zhu J, Wang H G and Zhang Z X 2021 Shape-tunable Janus micromotors via surfactant-induced dewetting *Langmuir* **37** 4964–70
- [225] Jurado-Sánchez B, Pacheco M, Rojo J and Escarpa A 2017 Magnetocatalytic graphene quantum dots Janus micromotors for bacterial endotoxin detection *Angew. Chem., Int. Ed.* **56** 6957–61
- [226] Wu X F, Ehehalt R, Razinskas G, Feichtner T, Qin J and Hecht B 2022 Light-driven microdrones *Nanotechnol.* **17** 477–84
- [227] Li J X, Sattayasamitsathit S, Dong R F, Gao W, Tam R, Feng X M, Ai S and Wang J 2014 Template electrosynthesis of tailored-made helical nanoswimmers *Nanoscale* **6** 9415–20
- [228] Miskin M Z, Cortese A J, Dorsey K, Esposito E P, Reynolds M F, Liu Q K, Cao M, Muller D A, Mceuen P L and Cohen I 2020 Electronically integrated, mass-manufactured, microscopic robots *Nature* **584** 557–61
- [229] Michel M, Taylor A, Sekol R, Podsiadlo P, Ho P, Kotov N and Thompson L 2007 High-performance nanostructured membrane electrode assemblies for fuel cells made by layer-by-layer assembly of carbon nanocolloids *Adv. Mater.* **19** 3859–64
- [230] Hu N, Sun M M, Lin X K, Gao C Y, Zhang B, Zheng C, Xie H and He Q 2018 Self-propelled rolled-up polyelectrolyte multilayer microrockets *Adv. Funct. Mater.* **28** 1705684
- [231] Yang L S, Meng H F, Chao Y C, Huang H C, Luo C W, Zan H W, Horn S F, Huang H L, Lai C C and Liou Y M 2020 The influence of the interfacial layer on the stability of all-solution-processed organic light-emitting diodes *RSC Adv.* **10** 28766–77

- [232] Yeh Y W *et al* 2021 Advanced atomic layer deposition technologies for micro-LEDs and VCSELs *Nanoscale Res. Lett.* **16** 164
- [233] De Ávila B E F *et al* 2017 Micromotor-enabled active drug delivery for *in vivo* treatment of stomach infection *Nat. Commun.* **8** 272
- [234] Şişman İ 2011 Template-assisted electrochemical synthesis of semiconductor nanowires *Nanowires—Implementations and Applications* ed A Hashim (InTech) pp 41–58
- [235] García-Torres J, Serrà A, Tierno P, Alcobé X and Vallés E 2017 Magnetic propulsion of recyclable catalytic nanocleaners for pollutant degradation *ACS Appl. Mater. Interfaces* **9** 23859–68
- [236] Lim J M, Bertrand N, Valencia P M, Rhee M, Langer R, Jon S, Farokhzad O C and Karnik R 2014 Parallel microfluidic synthesis of size-tunable polymeric nanoparticles using 3D flow focusing towards *in vivo* study *Nanomed. Nanotechnol. Biol. Med.* **10** 401–9
- [237] Zou M H, Wang J, Yu Y R, Sun L Y, Wang H, Xu H and Zhao Y J 2018 Composite multifunctional micromotors from droplet microfluidics *ACS Appl. Mater. Interfaces* **10** 34618–24
- [238] Love J C, Wolfe D B, Jacobs H O and Whitesides G M 2001 Microscope projection photolithography for rapid prototyping of masters with micron-scale features for use in soft lithography *Langmuir* **17** 6005–12
- [239] Brooks A M, Tasinkevych M, Sabrina S, Velegol D, Sen A and Bishop K J M 2019 Shape-directed rotation of homogeneous micromotors via catalytic self-electrophoresis *Nat. Commun.* **10** 495
- [240] Go G, Nguyen V D, Jin Z, Park J O and Park S 2018 A thermo-electromagnetically actuated microrobot for the targeted transport of therapeutic agents *Int. J. Control Autom. Syst.* **16** 1341–54
- [241] Kawata S, Sun H B, Tanaka T and Takada K 2001 Finer features for functional microdevices *Nature* **412** 697–8
- [242] Tottori S, Zhang L, Qiu F M, Krawczyk K K, Franco-Obregón A and Nelson B J 2012 Magnetic helical micromachines: fabrication, controlled swimming, and cargo transport *Adv. Mater.* **24** 811–6
- [243] Mohanty S, Paul A, Matos P M, Zhang J N, Sikorski J and Misra S 2022 CeFlowBot: a biomimetic flow-driven microrobot that navigates under magneto-acoustic fields *Small* **18** 2105829
- [244] Iacovacci V, Blanc A, Huang H W, Ricotti L, Schibli R, Mencias A, Behe M, Pané S and Nelson B J 2019 High-resolution SPECT imaging of stimuli-responsive soft microrobots *Small* **15** 1900709
- [245] Kucinski T M, Dawson J N and Freedman M A 2019 Size-dependent liquid–liquid phase separation in atmospherically relevant complex systems *J. Phys. Chem. Lett.* **10** 6915–20
- [246] Huang X, Liu Y, Feng A, Cheng X, Xiong X Y, Wang Z M, He Z X, Guo J T, Wang S and Yan X B 2022 Photoactivated organic nanomachines for programmable enhancement of antitumor efficacy *Small* **18** 2201525
- [247] Frank B D, Djalali S, Baryzewska A W, Giusto P, Seeberger P H and Zeininger L 2022 Reversible morphology-resolved chemotactic actuation and motion of Janus emulsion droplets *Nat. Commun.* **13** 2562
- [248] Kim S H, Mohseni P K, Song Y, Ishihara T and Li X L 2015 Inverse metal-assisted chemical etching produces smooth high aspect ratio InP nanostructures *Nano Lett.* **15** 641–8
- [249] Liang Z X and Fan D L 2018 Visible light–gated reconfigurable rotary actuation of electric nanomotors *Sci. Adv.* **4** eaau0981
- [250] Dai B H, Wang J Z, Xiong Z, Zhan X J, Dai W, Li C C, Feng S P and Tang J Y 2016 Programmable artificial phototactic microswimmer *Nat. Nanotechnol.* **11** 1087–92
- [251] Borah D, Shaw M T, Rasappa S, Farrell R A, O'mahony C, Faulkner C M, Bosea M, Gleeson P, Holmes J D and Morris M A 2011 Plasma etch technologies for the development of ultra-small feature size transistor devices *J. Phys. D: Appl. Phys.* **44** 174012
- [252] Bao J J, Yang Z, Nakajima M, Shen Y J, Takeuchi M, Huang Q and Fukuda T 2014 Self-actuating asymmetric platinum catalytic mobile nanorobot *IEEE Trans. Robot.* **30** 33–39
- [253] Dong Y, Yi C, Yang S S, Wang J, Chen P, Liu X, Du W, Wang S and Liu B F 2019 A substrate-free graphene oxide-based micromotor for rapid adsorption of antibiotics *Nanoscale* **11** 4562–70
- [254] Wang X Y, Feng X Y, Ma G P, Yao L and Ge M F 2016 Amphiphilic Janus particles generated via a combination of diffusion-induced phase separation and magnetically driven dewetting and their synergistic self-assembly *Adv. Mater.* **28** 3131–7
- [255] Ren M, Guo W L, Guo H S and Ren X H 2019 Microfluidic fabrication of bubble-propelled micromotors for wastewater treatment *ACS Appl. Mater. Interfaces* **11** 22761–7
- [256] Hussain M *et al* 2019 Biodegradable polymer microparticles with tunable shapes and surface textures for enhancement of dendritic cell maturation *ACS Appl. Mater. Interfaces* **11** 42734–43
- [257] Vilela D, Stanton M M, Parmar J and Sánchez S 2017 Microbots decorated with silver nanoparticles kill bacteria in aqueous media *ACS Appl. Mater. Interfaces* **9** 22093–100
- [258] Zhou J R *et al* 2021 Physical disruption of solid tumors by immunostimulatory microrobots enhances antitumor immunity *Adv. Mater.* **33** 2103505
- [259] Li J X, Singh V V, Sattayasamitsathit S, Orozco J, Kaufmann K, Dong R F, Gao W, Jurado-Sanchez B, Fedorak Y and Wang J 2014 Water-driven micromotors for rapid photocatalytic degradation of biological and chemical warfare agents *ACS Nano* **8** 11118–25
- [260] Venugopalan P L, Sai R, Chandorkar Y, Basu B, Shivashankar S and Ghosh A 2014 Conformal cyto-compatible ferrite coatings facilitate the realization of a nanovoyager in human blood *Nano Lett.* **14** 1968–75
- [261] Cao W X, Liu Y, Ran P, He J, Xie S, Weng J and Li X H 2021 Ultrasound-propelled Janus rod-shaped micromotors for site-specific sonodynamic thrombolysis *ACS Appl. Mater. Interfaces* **13** 58411–21
- [262] Yoshizumi Y and Suzuki H 2017 Self-propelled metal–polymer hybrid micromachines with bending and rotational motions *ACS Appl. Mater. Interfaces* **9** 21355–61
- [263] Fusco S *et al* 2015 Shape-switching microrobots for medical applications: the influence of shape in drug delivery and locomotion *ACS Appl. Mater. Interfaces* **7** 6803–11
- [264] Wang H, Chen X R, Meng X, He Y S, Jin B W, Zhao X L and Ye C H 2024 Soft micromotors with switchable motion enabled by 3D-to-3D shape reconfiguration *Chem. Mater.* **36** 4174–84
- [265] Baptista-Pires L, Orozco J, Guardia P and Merkoçi A 2018 Architecting graphene oxide rolled-up micromotors: a simple paper-based manufacturing technology *Small* **14** 1702746
- [266] Solovev A A, Mei Y F, Bermúdez Ureña E, Huang G S and Schmidt O G 2009 Catalytic microtubular jet engines self-propelled by accumulated gas bubbles *Small* **5** 1688–92
- [267] Xu B R, Zhang X Y, Tian Z A, Han D, Fan X C, Chen Y M, Di Z F, Qiu T and Mei Y F 2019 Microdroplet-guided intercalation and deterministic delamination towards intelligent rolling origami *Nat. Commun.* **10** 5019

- [268] Wu Z G, Lin X K, Wu Y J, Si T Y, Sun J M and He Q 2014 Near-infrared light-triggered “on/off” motion of polymer multilayer rockets *ACS Nano* **8** 6097–105
- [269] Dong R F, Wang C, Wang Q L, Pei A, She X L, Zhang Y X and Cai Y P 2017 ZnO-based microrockets with light-enhanced propulsion *Nanoscale* **9** 15027–32
- [270] Gao W, Feng X M, Pei A, Kane C R, Tam R, Hennessy C and Wang J 2014 Bioinspired helical microswimmers based on vascular plants *Nano Lett.* **14** 305–10
- [271] Li Z Q *et al* 2024 Multifunctional *Spirulina*-hybrid helical microswimmers: imaging and photothermal efficacy enabled by intracellular gold deposition *Chem. Eng. J.* **487** 150584
- [272] Yan X H *et al* 2015 Magnetite nanostructured porous hollow helical microswimmers for targeted delivery *Adv. Funct. Mater.* **25** 5333–42
- [273] Ceylan H, Dogan N O, Yasa I C, Musaoglu M N, Kulali Z U and Sitti M 2021 3D printed personalized magnetic micromachines from patient blood-derived biomaterials *Sci. Adv.* **7** eabh0273
- [274] Walker D, Käsdorf B T, Jeong H H, Lieleg O and Fischer P 2015 Enzymatically active biomimetic micropropellers for the penetration of mucin gels *Sci. Adv.* **1** e1500501
- [275] Ghosh A, Dasgupta D, Pal M, Morozov K I, Leshansky A M and Ghosh A 2018 Helical nanomachines as mobile viscometers *Adv. Funct. Mater.* **28** 1705687
- [276] Yu Y R, Shang L R, Gao W, Zhao Z, Wang H and Zhao Y J 2017 Microfluidic lithography of bioinspired helical micromotors *Angew. Chem.* **129** 12295–9
- [277] Jeon S *et al* 2019 Magnetically actuated microrobots as a platform for stem cell transplantation *Sci. Robot.* **4** eaav4317
- [278] Li D F, Liu C, Yang Y Y, Wang L D and Shen Y J 2020 Micro-rocket robot with all-optic actuating and tracking in blood *Light Sci. Appl.* **9** 84
- [279] Li D F, Liu Y T, Yang Y Y and Shen Y J 2018 A fast and powerful swimming microrobot with a serrated tail enhanced propulsion interface *Nanoscale* **10** 19673–7
- [280] Sun M M, Liu Q, Fan X J, Wang Y F, Chen W N, Tian C Y, Sun L N and Xie H 2020 Autonomous biohybrid urchin-like microporator for intracellular payload delivery *Small* **16** 1906701
- [281] Dong Y, Wang L, Yuan K, Ji F T, Gao J H, Zhang Z F, Du X Z, Tian Y, Wang Q Q and Zhang L 2021 Magnetic microswarm composed of porous nanocatalysts for targeted elimination of biofilm occlusion *ACS Nano* **15** 5056–67
- [282] Kiristi M, Singh V V, Esteban-fernández De Ávila B, Uygun M, Soto F, Aktaş Uygun D and Wang J 2015 Lysozyme-based antibacterial nanomotors *ACS Nano* **9** 9252–9
- [283] Chen W N, Sun M M, Fan X J and Xie H 2020 Magnetic/pH-sensitive double-layer microrobots for drug delivery and sustained release *Appl. Mater. Today* **19** 100583
- [284] Zhang H, Mourran A and Möller M 2017 Dynamic switching of helical microgel ribbons *Nano Lett.* **17** 2010–4
- [285] Luchnikov V, Kumar K and Stamm M 2008 Toroidal hollow-core microcavities produced by self-rolling of strained polymer bilayer films *J. Micromech. Microeng.* **18** 035041
- [286] Hahn V, Rietz P, Hermann F, Müller P, Barner-Kowollik C, Schlöder T, Wenzel W, Blasco E and Wegener M 2022 Light-sheet 3D microprinting via two-colour two-step absorption *Nat. Photon.* **16** 784–91
- [287] Fan Z Y, Gao R X, He Q B, Huang Y, Jiang T X, Peng Z K, Thévenaz L, Xiong Y Y and Zhong S C JDMD Editorial Office 2023 New sensing technologies for monitoring machinery, structures, and manufacturing processes *J. Dyn. Monit. Diagn* **2** 69–88
- [288] Mekid S and Bashmal S 2019 Engineering manipulation at nanoscale: further functional specifications *J. Eng. Des. Technol.* **17** 572–90
- [289] Gong Z, Chen B K, Liu J and Sun Y 2014 Robotic probing of nanostructures inside scanning electron microscopy *IEEE Trans. Robot.* **30** 758–65
- [290] Shi C Y, Luu D K, Yang Q M, Liu J, Chen J, Ru C H, Xie S R, Luo J, Ge J and Sun Y 2016 Recent advances in nanorobotic manipulation inside scanning electron microscopes *Microsyst. Nanoeng.* **2** 16024
- [291] Shang W F, Zhu M J, Ren H and Wu X Y 2020 Centering of a miniature rotation robot for multi-directional imaging under microscopy *IEEE Trans. Nanotechnol.* **19** 17–20
- [292] Jin Z Q, Zhang Z Z and Gu G X 2019 Autonomous in-situ correction of fused deposition modeling printers using computer vision and deep learning *Manuf. Lett.* **22** 11–15
- [293] Yang L D, Jiang J L, Ji F T, Li Y M, Yung K L, Ferreira A and Zhang L 2024 Machine learning for micro- and nanorobots *Nat. Mach. Intell.* **6** 605–18